A Python approach for GRB afterglow analysis: sAGa (Software for AfterGlow Analysis)

Marco Marongiu[1,2], Cristiano Guidorzi [2,3,4]

[1] INAF - Osservatorio Astronomico di Cagliari, via della Scienza, 5 - 09047 Selargius (CA), Italia

[2] Dipartimento di Fisica e Scienze della Terra, Università di Ferrara, via Saragat, 1 - 44122, Ferrara, Italia

[3] INFN - Sezione di Ferrara, via Saragat, 1 - 44122, Ferrara, Italia

[4] INAF - Osservatorio di Astrofisica e Scienza dello Spazio di Bologna, via Piero Gobetti, 101 - 40129 Bologna, Italia

Abstract

This technical note describes a fully self-consistent code in Python – called sAGa (Software for AfterGlow Analysis) – to cope with the complex landscape of GRB afterglows. sAGa adds up to other pre-existing broadband fitting tools in the literature and provides an independent check, emphasising the broadband study of GRB afterglows over the last two decades.

This code aims to model GRB afterglow data within a self-consistent physically grounded picture. Built adopting a Bayesian approach, all the data set, from radio to gamma-rays, is modelled. By-products are plots of spectra and light-curves, and computation of the break frequencies and normalisations as a function of the shock microphysical parameters, such as the power-law index of the electron energy distribution, the fractions of the blastwave energy delivered to relativistic electrons and magnetic fields, and other parameters such as the kinetic energy of the explosion and the density of the circumburst medium (CBM). Dust extinction of optical along the sightline and scintillation in radio frequencies are also accounted for.

sAGa has been successfully tested on the broadband data of the afterglows of GRB 120521C, GRB 090423, and GRB 050904. Our results are consistent with those reported in the literature within $\lesssim 2\sigma$. Moreover, the values of the power-law index of the electron energy distribution obtained from sAGa analysis are compatible with the inferences based on the lines of reasoning based on the observation of the optical/X-ray spectra.

This INAF Technical Note was created with LaTeX.

Contents

1 Introduction: an analytical approach for broadband modelling of GRB afterglows

The afterglow radiation from gamma-ray bursts (GRBs) – short and intense pulses of gamma-ray radiation, originating from either core collapsing massive stars (e.g. [149]) or binary neutron star (BNS) mergers (e.g. [1]) – takes place when the outflow from the GRB central engine penetrates the circumburst medium (CBM), resulting mainly in synchrotron radiation (for a review see e.g. [102, 83, 31]). It originates in two shock regions: a forward shock (FS) that propagates in the CBM (e.g. [44], hereafter GS02), and a reverse shock (RS) that propagates back into the flow itself and radiates at lower frequencies (e.g. [85, 57, 59, 32]).

GRB afterglows encode a wealth of information on (1) the radiation mechanism, in particular the possible presence of large-scale magnetic fields ploughing the ejecta, which is still one of the main open issues in the field (e.g. [51]); (2) relativistic shock micro-physics; (3) energetics; (4) jet geometry. All these issues can be addressed effectively and uniquely through observations at lower frequencies, especially in the radio band. Observations of radio afterglows are key to diagnose the GRB physics (e.g. [90]), especially for the understanding of the RS component, which links directly to the nature of the outflow and, consequently, to the progenitor itself (e.g. [60]). On the other hand, the detection of radio afterglows has proven challenging with current radio telescopes (e.g. [13]) – especially in single-dish mode [80] – mainly because of their faintness ($\lesssim$ mJy).

The analysis of GRB afterglow spectra and light curves is made possible using data from radio to X-ray frequencies. The ongoing improvements in sensitivity for broadband facilities, especially at radio frequencies – such as the upgraded Giant Metre-wave Radio Telescope (GMRT, [130, 54, 45])[1], the Karl G. Jansky Very Large Array (VLA, [133])[2], the Arcminute Microkelvin Imager Large Array (AMI-LA, [162])[3], and the NOrthern Extended Millimeter Array (NOEMA, [15])[4] – give the opportunity to gain insight into the micro-physical parameters with unprecedented accuracy. In parallel, the continuous evolution of computational resources fosters the development of sophisticated data analysis packages (e.g. [109, 56, 22, 62, 12, 159, 138, 151, 137, 23, 42, 68, 69, 111, 3, 114, 6]), but to date there is no computational tool that is able to fully describe the complex landscape of the GRB afterglows.

In this context we developed a fully self-consistent code in Python called sAGa (Software for AfterGlow Analysis), described in this technical note. sAGa provides an independent tool among other computational packages aimed at broadband modelling of GRB afterglows. Built adopting a Bayesian approach, all the data, from radio to gamma-rays, are modelled. sAGa considers different radiation processes (synchrotron and inverse Compton radiation, Sects. 4 and 9, respectively), and other aspects, described in this technical note (jetted emission and non-relativistic regime, Sect. 5; energy injection phenomenon, Sect. 6; extinction and absorption effects, Sect. 7; scintillation in radio frequencies, Sect. 8), selectable by the user through a simple widget displayed when sAGa is launched.

This application receives in input two text-based files (Sect. 2.2): the "observation data file" (a table containing the epoch of observation, the flux density and its uncertainty, and the observing frequency) and the GRB "parameter file" (such as the sky position and the redshift). Later, sAGa performs a broadband data analysis in a single process through a

[1] http://www.gmrt.ncra.tifr.res.in/
[2] https://science.nrao.edu/facilities/vla
[3] https://www.astro.phy.cam.ac.uk/research/research-projects/AMI
[4] http://iram-institute.org/EN/noema-project.php

new approach that consists in the manipulation of all the data both at each given epoch and given frequency. Finally, in output sAGa provides several plots of light curves and spectra of the GRB afterglow (both for each epoch/observing frequency and global) and a text-based file reporting best-fit values associated with the user's configuration (selected radiation processes and other aspects).

sAGa determines the break frequencies and normalisations as a function of the shock microphysical parameters, such as the power-law index of the electron energy distribution (p), the fractions of the blastwave energy delivered to relativistic electrons (ϵ_e) and magnetic fields (ϵ_B), and other parameters such as the kinetic energy of the explosion ($E_{K,\rm iso}$), and the CBM density (n_0 for ISM-like CBM; the normalised mass-loss rate A_* for wind-like CBM). Dust extinction of optical along the sightline is also accounted for in terms of the V-band extinction A_V.

sAGa has been successfully tested on the broadband data of the afterglows of GRB 120521C, GRB 090423, and GRB 050904 for which analogous and independent analyses are available in the literature, where the results obtained with sAGa are consistent with those reported in the literature (especially [67], hereafter L14, who make use of a similar approach for the characterisation of the GRB afterglow) within $\lesssim 2\sigma$.

This technical note is organised as follows. Preliminary information about sAGa is reported in Sect. 2; the Markov Chain Monte Carlo (MCMC) analysis in Bayesian approach – crucial in high-dimensional problems (like the present one) – is reported in Sect. 3; the physical aspects of GRB afterglow emission encoded in sAGa are described in Sects. 4, 5, 6, 7, 8, 9. The test phase of sAGa on other GRB afterglows is reported in Sect. 10, and finally we give our conclusions in Sect. 11.

Hereafter, sAGa assumes default ΛCDM cosmological parameters of $\Omega_m = 0.32$, $\Omega_\Lambda = 0.69$, and $H_0 = 67.4$ km s^{-1} Mpc^{-1} [103]; the user can use specific tools available in the Python Astropy package[5] [5, 104] to customise these parameters.

[5] https://www.astropy.org/

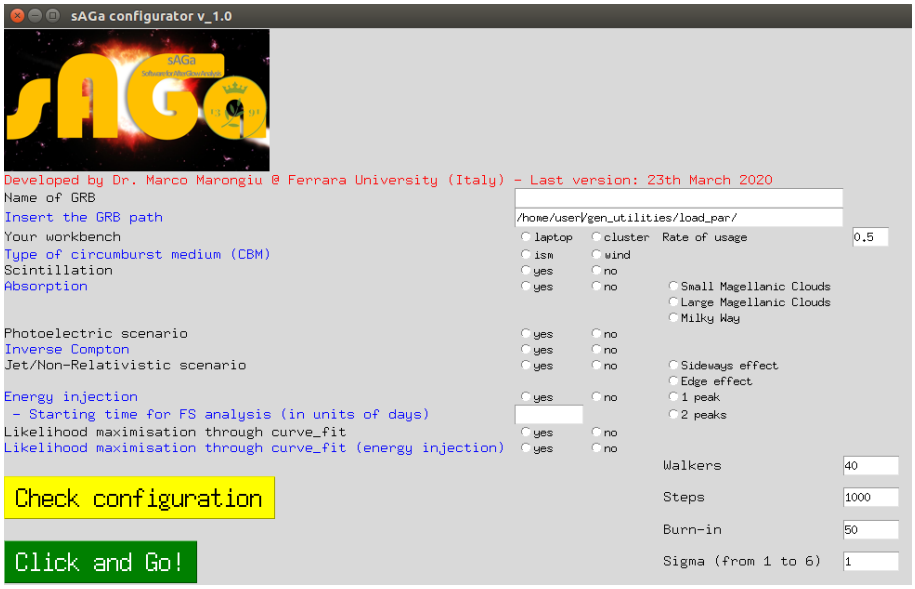

Figure 1: *Widget of* sAGa. *The user must compile all the boxes before clicking the button "Click and Go!".*

2 Preliminary information

sAGa is compatible with the following characteristics:

- Ubuntu 12.04 (x32 or x64-based operating system) or recent versions as operating system;
- 4 GB or more of RAM (16 GB recommended);
- 5 GB or more of free disk space;
- python 3.X.X;
- emcee 3.X.X;
- anaconda 4.X.X or more.

2.1 Usage of sAGa

The usage of sAGa is very simple, thanks to a very intuitive widget (Fig 1). After filling the form with the required details for the analysis, the "Check configuration" yellow button allows to verify the configuration on the user's terminal, and eventually to modify the configuration. Once satisfied with the selected configuration, the "Click and Go!" green button launches sAGa.

2.2 Preparation of data files

Before using sAGa, the user must compile three text-based files:

1. The *data tables* – one for each observing frequency – contain the data set of the GRB afterglow under consideration; each table must include (1) the epoch of observation (in units of days), (2) the flux density and (3) its uncertainty (in units of mJy), (4) the

observing frequency (in units of Hz), and (5) the nature of the measure (0 for upper limit, 1 for detection). These tables are stored in a working directory that the user must type in the "Insert the GRB path" box of the widget (Fig. 1).

2. The *"observation data file"* includes the necessary instructions for reading the data tables from sAGa.

3. The *"parameter file"* contains all the known information about the GRB afterglow under consideration, such as the GRB position and its redshift.

2.3 Composition of sAGa

sAGa consists in a sophisticate Python architecture (Fig. 2), composed of several environments:

- **importlibmod.py** ⇒ This part acquires the information from the text-based files described in Sect. 2.2.
- **maths.py** ⇒ Some mathematical/statistical functions are contained in this file.
- **bayesian.py** ⇒ In this file there are the necessary functions for the Bayesian analysis of the data.
- **scint.py** ⇒ This part includes the functions related to the radio scintillation analysis (for further information see Sect. 8).
- **absorp_opt.py - nh_photo.py** ⇒ All the functions responsible for the dust extinction in optical and the photoelectric absorption in X-rays (see Sect. 7) are included in this file.
- **jet_nr.py** ⇒ In this file there is the part regarding the jetted emission and the Newtonian regime (Sect. 5).
- **class_fs.py - class_ei.py - class_rs.py** ⇒ All the functions describing the radiation mechanisms ascribed to forward (FS) and reverse shocks (RS)[6] and the energy injection regime (Sect. 6) are contained in these files.
- **inv_compton.py** ⇒ This part regards the inverse Compton radiation, nearing completion (Sect. 9).
- **plot_fit_synchr.py** ⇒ This is the output of sAGa, containing the functions for the production of spectra and light curves (Sect. 4, both plots and tables), and Bayesian/modelling results (Sect. 3). The output is located in the directory path typed from the user in the "Insert the GRB path" box in the widget (Fig. 1).

3 Markov Chain Monte Carlo

The best-fit solution for a data set sAGa that includes both detections and upper limits, is calculated through the maximisation of the following likelihood function, given by (e.g., L14):

$$\prod p(e_i)^{\delta_i} F(e_i)^{1-\delta_i} \tag{1}$$

[6] Reverse shock regime is incomplete and currently unavailable.

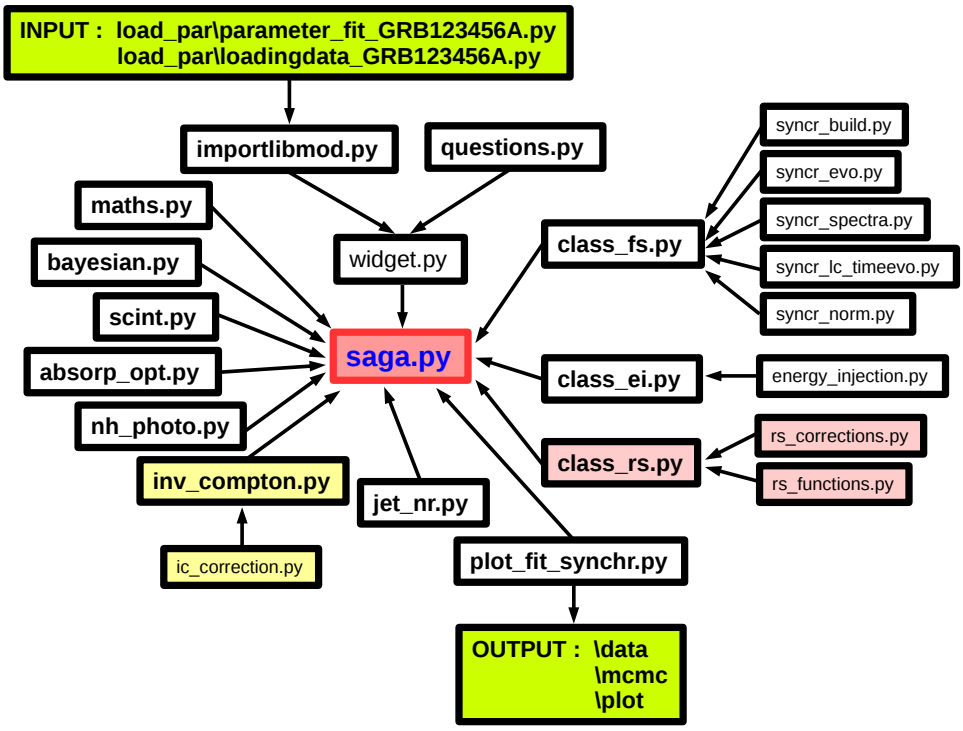

Figure 2: *Structure of* sAGa. *Yellow boxes indicate the sections nearing completion; red boxes indicate the incomplete parts. Input/Output are labeled in green.*

where e_i are the residuals (the difference between either measurement or 3σ upper limit and the predicted flux from the model), δ_i is the detection parameter (equal to 0 for a 3σ upper limit and 1 for a detection), $p(e_i)$ is the probability density function of the residuals (we assumed a Gaussian error model), and $F(e_i)$ is the cumulative distribution function of the residuals. In sAGa the maximisation of the likelihood function is calculated by using the sequential least squares programming tool available in the Python SciPy package[7] [50].

The radiation processes and other additional aspects involved in sAGa inevitably introduce many free parameters (Table 1): in this high-dimensional problem the algorithm would be stuck in local minima. This can be overcome through a Markov Chain Monte Carlo (MCMC) analysis in Bayesian approach (e.g. [125, 81]) using the Python-based code emcee[8] [26]: the model parameters are constrained through the definition of prior distributions that encode preliminary and general information; the respective parameter space for each model parameter is derived from accurate modelling of the broadband GRB afterglows (e.g., [124, 68, 117, 100, 126, 64]), and is reported in Table 1. sAGa considers (1) uniform priors for the parameters that describe the exponential terms on the flux densities (A_V) and the power-law indices (p and the injection index m; Sect. 6), and (2) Jeffreys priors [49], for the parameters that span different orders of magnitudes ($E_{K,\rm iso}$, n_0, A_*, ϵ_e, ϵ_B and t_j). ϵ_e and ϵ_B are currently believed to be of the order of a few percent to tens of percent by energy [127]; therefore, their priors are truncated at an upper bound of 1/3, corresponding to their expected equipartition values (e.g. L14)[9].

[7] http://www.scipy.org/
[8] https://emcee.readthedocs.io/en/stable/
[9] This consists in the equal distribution of the internal energy among the magnetic field, the accelerated

Table 1: *Free parameter space available in* SAGA*, with relative range of definition (for further details, see Sect. 3).*

Parameter	Unit	Description	Range definition
p	-	Power-law index of the electron energy distribution	1.5 – 3.5
ϵ_e	-	Blastwave energy rate delivered to relativistic electrons	0 – 1/3
ϵ_B	-	Blastwave energy rate delivered to magnetic fields	0 – 1/3
$E_{K,\rm iso}$	10^{52} erg	Kinetic energy of the explosion (in units of 10^{52} erg)	10^{-2} – 10^{3}
n_0	cm^{-3}	Density for ISM-like CBM	10^{-3} – 10^{2}
A_*	5×10^{11} g cm^{-1}	Parameter connected with the wind-like density CBM	10^{-3} – 10^{2}
A_V	mag	Extinction in the host galaxy	0 – 10
t_j	d	Jet break time	According to the case
$t_{ei,1}$	d	Beginning time of the first injection	According to the case
$t_{ei,2}$	d	Beginning time of the second injection	According to the case
m, m_2	-	Injection indices (m_2 in case of two bumps)	0 – 3 (ISM)
m, m_2	-	Injection indices (m_2 in case of two bumps)	0 – 1 (wind)

In the MCMC analysis the ensemble sampler is initially run until the convergence of the average likelihood across the chains; the initial (unstable) period, called "burn-in", is discarded (recommended Markov chains for this phase: 500). The subsequent Markov chains are set up between 10^3 and 10^4, depending on both the complexity of the problem and the computational characteristics. As reported by L14, the convergence is checked by verifying the stability (over the length of the chain following burn-in) of the distributions; these distributions frequently exhibit long tails, and hence the quantiles are referred to compute summary statistics and quote 68% credible regions around the median. All these MCMC parameters are selectable with SAGA in the widget (Fig. 1, on the lower right) through the "*Walkers*"[10], "*Steps*", "*Burn-in*", and "*Sigma*"[11] boxes; the user must be aware that high values of *Steps* ($> 10^4$) correspond to high computational performance[12].

4 GRB synchrotron emission

GRB afterglow radiation is thought to be the result of the relativistic ejecta being slowed down by the surrounding CBM [84] and takes place when a significant rate of the ejecta energy is transferred to the shocked external medium. At the early-stage of the GRB afterglow (about the first few hours), the radiative processes are responsible of the loss of a significant fraction of the kinetic energy; later, in the adiabatic phase, the radiation losses become negligible [102].

The hydrodynamics of the adiabatic phase, and the resulting synchrotron emission, is based on the theory of relativistic blastwaves [11]; this theory consists in a self-similar spherical solution for an adiabatic ultra relativistic blastwave characterised by a Lorentz factor of the shocked fluid (also known as blastwave Lorentz factor) $\Gamma \gg 1$. The electrons are accelerated to relativistic speed by the 1st-order Fermi acceleration mechanism, which implies a power-law distribution in terms of energy, given by:

$$N(\gamma_e)d\gamma_e \propto \gamma_e^{-p} d\gamma_e \tag{2}$$

where γ_e is the electron Lorentz factor, and p is the electron energy distribution power-law index, usually ranging between constrained to 1.5 and 3.5 ([44], hereafter GS02).

electrons and the baryons (protons/neutrons).

[10] The user must choose an even integer; the minimum value corresponds to twice as the number of parameters, plus 2.

[11] We quoted the uncertainties based on the quantiles – in terms of sigma – of the samples in the marginalised distributions.

[12] For further details, see https://emcee.readthedocs.io/en/stable/tutorials/line/.

The minimum injected electron Lorentz factor γ_m ($< \gamma_e$) in this distribution is defined as:

$$\gamma_m = \Gamma \epsilon_e \left(\frac{p-2}{p-1}\right) \frac{m_p}{m_e} \tag{3}$$

where m_e and m_p are the electron mass and the proton mass, respectively. In the presence of the self-generated magnetic fields, these relativistic particles lose their energy emitting synchrotron radiation. The typical synchrotron frequency of a relativistic electron depends on its Lorentz factor and – in the observer frame – is given by:

$$\nu(\gamma_e) \simeq \Gamma \gamma_e^2 \frac{q_e B}{2\pi m_e c} \tag{4}$$

where q_e is the electron charge; B is the comoving magnetic field strength.

The spectral power of a relativistic electron P_ν with initial energy $\gamma_e mc^2$ varies approximately as $\nu^{1/3}$ for $\nu < \nu(\gamma_e)$ and cuts off exponentially for $\nu > \nu(\gamma_e)$. The total emitted power can be expressed – in the observer frame – as:

$$P(\gamma_e) \simeq \frac{4}{3} \sigma_T c \Gamma^2 \gamma_e^2 \frac{B^2}{8\pi} \tag{5}$$

where σ_T is the electron Thomson cross-section. The total peak spectral power $P_{\nu,max} \approx P(\gamma_e)/\nu(\gamma_e)$ is independent of γ_e and occurs at $\nu(\gamma_e)$.

This picture is valid only in adiabatic phase, where the electron radiates a negligible fraction of its energy, and hence until γ_e is less than a critical Lorentz factor γ_c:

$$\gamma_c = \frac{6\pi m_e c}{\Gamma \sigma_T B^2 t} \,, \tag{6}$$

where t is the timescale (in the observer-frame) within which an electron characterised by an initial Lorentz factor $\gamma_e > \gamma_c$ cools down to γ_c. Above γ_c, cooling by synchrotron radiation becomes significant, so that the shape of the electron distribution is modified in the $\gamma_e > \gamma_c$ regime [121, 31]. The electron Lorentz factors γ_m and γ_c – evolving in time – define two characteristic emission frequencies ν_m and ν_c in the synchrotron spectrum. Depending on the order of γ_m and γ_c, the synchrotron spectrum falls into two broad categories: fast-cooling ($\nu_m > \nu_c$, or $\gamma_m > \gamma_c$) and slow-cooling ($\nu_m < \nu_c$, or $\gamma_m < \gamma_c$) regimes. In the first case, all electrons with Lorentz factors above γ_c cool rapidly; in the second case, only the most energetic electrons cool rapidly (e.g., GS02, [121, 31]). The prompt phase of GRBs is expected to be in the fast-cooling regime [101], whereas the transition to the slow-cooling regime is expected to take place during the early stages of the afterglow ([84, 147], GS02).

Another characteristic frequency is the synchrotron self-absorption ν_{sa}, below which the synchrotron photons are self-absorbed (e.g. [119, 58]). During the afterglow phase, ν_{sa} is usually the smallest among the three frequencies. In particular, only in fast-cooling regime the self-absorption frequency splits in ν_{ac} and ν_{sa}, where an optical depth of unity is produced by noncooled electrons and all electrons, respectively ([43], GS02). When $\nu_{sa} > \nu_c$, the electron energy distribution may be significantly modified, resulting in inaccurate analytical models [31].

4.1 Evolution of GRB synchrotron spectra and light curves in sAGa

The synchrotron spectrum evolves with time as the blastwave expands, with spectral transitions occurring when two or more break frequencies cross each other. For the case of

FS emission, sAGa modelled the synchrotron broadband spectrum with smoothly connected power-law segments, following the prescriptions described in GS02. Such a model includes synchrotron cooling and self-absorption for both ISM and wind-like CBM, resulting in 5 different spectral regimes at any given time with 11 definitions of the break frequencies – corresponding to different combinations of the synchrotron frequencies – with the time-independent micro-physics parameters $E_{K,iso}$, p, n_0 (or A_*), ϵ_e and ϵ_B as free parameters (see Fig. 1 in GS02).

The synchrotron light curve at a given ν_{obs} evolves with time, undergoing temporal transitions (or power-law breaks) whenever a characteristic frequency crosses ν_{obs}. This translates in smoothly connected power-law segments: for example, t_m and t_c are the times at which ν_m and ν_c cross ν_{obs}, respectively, that is $\nu_m(t_m) = \nu_c(t_c) = \nu_{obs}$. As described in [121], the possible orderings of break times depend on the comparison between ν_{obs} and $\nu_0 = \nu_c(t_0) = \nu_m(t_0)$, where t_0 is the transition time between fast and slow cooling regimes. The regime $\nu_{obs} > \nu_0$ defines the high-frequency light curve, where $t_0 > t_m > t_c$; on the other hand, the regime $\nu_{obs} < \nu_0$ defines the low-frequency light curve, characterised by $t_0 < t_m < t_c$. In sAGa light curves are calculated through a specific time-dependent weighting scheme described in L14; the transition time t_{trans} between different spectral regimes is calculated through geometric average, since sometimes in GS02 the same t_{trans} is defined by different equations.

5 Jetted emission and non-relativistic transition

In their work, the hydrodynamics presented by GS02 assumes isotropic expansion; however, the GRB outflow usually shows evidence for the presence of a jetted emission in the form of an achromatic break in the temporal power-law decay of the afterglow light curves. This is usually interpreted as the edge of the jet becoming visible to the observer.

In the literature there are two broad families of jets: uniform and structured. The first assumes an uniform distribution of energy and Lorentz factor within a jet cone with a sharp edge (the so-called "top-hat jet"), the second assumes an angular distribution in energy and Lorentz factor (e.g. [37, 152]). sAGa considers the uniform jet regime, because is simpler than structured jet model, based on special relativistic hydrodynamics (e.g. [23, 40, 18]); although in the latest years the growing evidence has been found that favours the structured jet, as in the case of the GRB 170817A associated to GW 170817 [4][13]

The uniform jet scenario, based on purely geometrical or dynamical effects, assumes a simplified conical jet blastwave, with a half opening angle θ_j and Γ, where only the emission inside the $1/\Gamma$ cone is detectable due to relativistic beaming. During the deceleration phase – for an observer in the jet sightline – Γ decreases gradually until $1/\Gamma > \theta_j$ in the form of an achromatic jet break at the jet break time t_j[14]. The light curve steepening can arise from two effects: the pure edge effect (e.g. [97]) and the sideways expansion effect [109, 120]. In the pure edge effect, the blastwave dynamics does not change during the jet break transition; the degree of steepening at t_j for the flux densities is defined as $\Delta\alpha = \alpha_{post,jet} - \alpha_{pre,jet} = (3-k)/(4-k)$, where k is the exponent of the density profile

[13] Recently, the open-source Python package afterglowpy is available for on-the-fly computation of structured jet afterglows with arbitrary viewing angle [114].

[14] However, afterglow observations in the Swift era have shown a lack of achromatic breaks compared to the pre-Swift era [24]. Missing breaks are attributed to far off-axis observations [142], to poor quality of data [20], or to the break time falling beyond the end of Swift/XRT follow-up. Another possible interpretation is that the X-ray afterglow of many GRBs does not originate from external shocks but from a long-lasting central engine [86], suggesting that only the optical light curve may be suitable to identify jet breaks.

$n = A\,r^{-k}$ ($k = 0$ for ISM-like CBM, $k = 2$ for wind-like CBM, [37]). The sideways expansion effect of a conical jet, as opposed to the pure edge effect, implies that the jet exponentially decelerates when $\Gamma \sim \theta_j^{-1}$; this feature translates in the change of the evolution of both the spectral break frequencies and flux densities at t_j, as described in several papers (e.g. [120, 122, 96]) and summarised in Table 5. Several numerical simulations and sophisticated analytical treatments suggest that the contribution of sideways expansion is significant up to $\Gamma \gtrsim 2$ [38, 62, 12, 159, 42, 23, 140], even if $\alpha = -p$ post-jet-break decay could be a reasonable rough approximation [152].

θ_j is computed, both for ISM-like and wind-like CBM, from t_j (expressed in units of days) [147, 109, 120, 16, 145] as:

$$\theta_{j,\rm ISM} = 9.25 \left(\frac{n_0}{E_{52,k,\rm iso}}\right)^{1/8} \left(\frac{t_j}{1+z}\right)^{3/8} \ \rm deg \tag{7}$$

$$\theta_{j,\rm wind} = 11.55 \left[\frac{t_j A_*}{(1+z)E_{52,k,\rm iso}}\right]^{1/4} \ \rm deg\ , \tag{8}$$

where z is the redshift of the source, $E_{52,k,\rm iso}$ is the isotropic-equivalent kinetic energy expressed in units of 10^{52} erg, n_0 is the number density in units of cm^{-3}, and A_* in units of 5×10^{11} g/cm [15]. For long GRBs, θ_j usually ranges between 3° and 10° (e.g., [10]): this results in a beaming correction factor $f_b = 1 - \cos\theta_j$ between $\sim 10^{-3}$ and $\sim 10^{-2}$, suggesting that the true released energy is two or three orders of magnitude lower than the measured $E_{\rm iso}$ (with a typical value of a few 10^{51} erg). On the other hand, measurements of θ_j for short GRBs are less frequent, mainly because of the faintness of their afterglows; the average θ_j of short GRBs seems to be larger than that of long GRBs [10, 25], with beaming-corrected energies usually lower than 10^{50} erg.

This picture is valid only for an on-axis observer, but the light curve behaviour also depends on the direction of the observer. Fitting X-ray data at late-time with numerical jet models suggests that the sightline for most GRBs is misaligned from the jet axis [113, 156]. For an off-axis observer, an orphan afterglow (characterised by the absence of the high-energy component) could in principle be observed at late-times. Several authors discussed the possibility of detecting orphan afterglows (e.g., [110, 92, 134, 161]). Recently [77] discovered a good candidate for an orphan afterglow of a long GRB in the radio transient source FIRST J1419+3940, characterised by decreasing brightness over the last few decades.

Finally, besides these two forms of jets, more complicated structured jets have been discussed in the literature, such as the two-component jet model. According to this model, the GRB outflow consists in a narrow jet component (usually characterised by a higher $L_{\gamma,\rm iso}$ and a larger Γ), surrounded by a wider jet component (with a lower $L_{\gamma,\rm iso}$ and a smaller Γ). Depending on the viewing angle, the two-component jet predicts some light curve features, such as an early jet break and late-time re-brightening [48, 99, 150]. This model was used to interpret the afterglow data for several GRBs, such as GRB 030329 [9] and GRB 080319B [105]. Moreover, this can be accommodated with the collapsar model, where a narrow and highly relativistic jet emerging from a star is surrounded by a wider, less relativistic cocoon [106, 153].

The relativistic blastwave, thanks to the interaction with the CBM, gradually decelerates, reaching the non-relativistic/Newtonian (NR) phase, when $\gamma < \sqrt{2}$ and the electrons should

[15] In the density profile $\rho(r) = Ar^{-2}$, r is the radius, $A = \dot{M}_w 4\pi V_w \equiv 5 \times 10^{11} A_*$ g cm^{-1} is a constant proportional to the progenitor mass-loss rate $\dot{M}_w$ (assumed constant), for a given wind velocity $V_w = 10^3$ km s^{-1} and $\dot{M}_w = 10^{-5}$ M$_\odot$ yr^{-1} [16].

be in the slow cooling scenario ($\nu_m < \nu_c$), at the transition time

$$t_{\rm NR,ISM} = 84(1+z)\left(\frac{E_{52,k,\rm iso}}{n_0}\right)^{1/3} \ \text{days} \tag{9}$$

for ISM-like CBM [147], and

$$t_{\rm NR,wind} = 694(1+z)\left(\frac{E_{52,k,\rm iso}}{A_*}\right) \ \text{days} \tag{10}$$

for wind-like CBM [16].

In the deep Newtonian phase, the blastwave dynamics can be derived from simple scaling relations (e.g. [148]). The light curves in the NR phase are steeper than those in the relativistic phase, but are shallower than the post-jet-break phase in the relativistic regime [152]. This feature suggests that the transition from relativistic to NR phase occurs after the jet break, probably in timescales of years (e.g. [74, 159]). This holds for ISM-like environment at the late stage of the blastwave evolution, since a stellar wind ends at a termination shock beyond which the medium is already of ISM type [31, 152].

Observationally, in the optical band it is very difficult to observe the NR phase in the light curves, since the afterglow emission is strongly contaminated by the host galaxy light before reaching the NR phase. On the other hand, this transition may be more easily observed in the radio band at late-time (timescales of years), especially in the case of nearby sources (e.g. GRB 030329, [136]).

sAGa is configured so that, at the beginning of the analysis, the user can select the jet/NR regime; this choice modifies the evolution of the spectral break frequencies and flux densities at t_j (free parameter) and t_{NR}, smoothing over the transition with a fixed smoothing parameter ($s = 5$, [38]). For completeness, the post-break (sideways expansion) and Newtonian evolution of the spectral break frequencies are reported in Table 5, following prescriptions reported in several works ([120, 30, 96, 122, 139, 70], GS02).

6 Energy injection

As the shock propagates into the CBM, the blastwave decelerates: this is observed through the decay evolution in the observed light curves of GRB afterglows. Sometimes, these light curves are characterised by plateaus, probably due to the re-brightening of the GRB afterglow (e.g. [93, 73, 78, 47]). This effect consists of the energy injection into the blastwave shock, the nature of which is explained through different possible mechanisms (e.g. [158, 41, 33]).

In the models based on the long-lasting central engine, such as a spinning-down millisecond magnetar [21, 157], the blastwave is fed by a long-lasting Poynting-flux-dominated wind, defined by the power-law decay with time:

$$L(t) = L_0\left(\frac{t}{t_0}\right)^{-q} \tag{11}$$

where t is the central engine time (corresponding to the observer time of GRB afterglow), L_0 is the luminosity at the reference time t_0, and $q \geq 0$[16]. This corresponds to the temporal evolution of the blastwave energy $E \propto t^{1-q} = t^m$, where $m = 1 - q$ is the "injection index".

[16] The same approach sometimes is based on $L(t) = L_0(t/t_0)^q$ and $q \leq 0$ (e.g. [87, 82, 141, 66]).

An alternative type of energy injection occurs when the central engine injects a stratified ejecta with a continuous distribution of bulk Lorentz factor γ, defined as the ejecta mass above a certain Lorentz factor [107, 118, 135]:

$$M(>\gamma) = \gamma^{-s} \, . \tag{12}$$

The ejecta is moving between a maximum γ_{max} – corresponding to the Lorentz factor of the blastwave at the onset of energy injection $t_{0,ei}$, $\Gamma(t_{0,ei})$ – and a minimum Lorentz factor γ_{min}. As the blastwave decelerates, energy injection takes place when $\Gamma(t_{0,ei}) \approx \gamma_{max}$ and hence the slower ejecta shells begin depositing energy into the blastwave. This regime lasts until the lowest energy ejecta located at γ_{min} have transferred their energy to the blastwave. Later, the afterglow proceeds like a standard regime, but powered by a blastwave with increased energy and Lorentz factor γ_{min}.

These two energy injection mechanisms can be considered equivalent through the connection between two injection parameters s and q as follows [154]:

$$s = \frac{10 - 3k - 7q + 2kq}{2 + q - k} \tag{13}$$

$$q = \frac{10 - 2s - 3k + ks}{7 + s - 2k} \, . \tag{14}$$

where k is the exponent of the density profile $n = A\, r^{-k}$ ($k = 0$ for ISM-like CBM, and $k = 2$ for wind-like CBM). From Eq. (14) follows that

$$m = \frac{(3-k)(s-1)}{7 + s - 2k} \, , \tag{15}$$

where m ranges between 0 and 3 for ISM-like CBM (between 0 and 1 for wind-like CBM). Moreover, s is bounded 1 and ∞ for both ISM-like CBM and wind-like CBM. In the absence of energy injection, the standard hydrodynamic evolution requires that $m = 0$, $s = 1$ or $q = 1$ in the above expressions (e.g. [31]).

sAGA accounts for energy injection – ranging between $t_{ei,i}$ and $t_{ei,f}$[17] (in units of days) – selecting the number of "bumps" of injected energy from the central engine (1 or 2)[18]. The kinetic energy in the standard afterglow regime (e.g. GS02) is modified in time according to the following broken power-law function [66]:

$$E_{52,k,iso}(t) = \begin{cases} E_{52,k,iso,f} & t \geq t_{ei,f} \\ E_{52,k,iso,f} \left(\frac{t}{t_{ei,f}}\right)^{m} & t_{ei,i} < t < t_{ei,f} \\ E_{52,k,iso,i} \equiv E_{52,k,iso,f} \left(\frac{t_{ei,i}}{t_{ei,f}}\right)^{m} & t \leq t_{ei,i} \end{cases} \tag{16}$$

for one bump of energy injection, where $E_{52,k,iso,i}$ and $E_{52,k,iso,f}$ are the initial and final blastwave energy (in units of 10^{52} erg), respectively, and

$$E_{52,k,iso}(t) = \begin{cases} E_{52,k,iso,f} & t \geq t_{ei,f} \\ E_{52,k,iso,f} \left(\frac{t}{t_{ei,f}}\right)^{m_1} & t_{ei,i_2} < t < t_{ei,f} \\ E_{52,k,iso,f} \left(\frac{t_{ei,i_2}}{t_{ei,f}}\right)^{m_1} \left(\frac{t}{t_{ei,i_2}}\right)^{m_2} & t_{ei,i_1} < t \leq t_{ei,i_2} \\ E_{52,k,iso,f} \left(\frac{t_{ei,i_2}}{t_{ei,f}}\right)^{m_1} \left(\frac{t_{ei,i_1}}{t_{ei,i_2}}\right)^{m_2} & t \leq t_{ei,i_1} \end{cases} \tag{17}$$

[17] This parameter is fixed by the observer and obtained by independent modelling of broadband light curves.

[18] This number will be implemented for higher values.

for two consecutive bumps of energy injection, where m_1 and m_2 are the injection indices referred to the first and second bump, respectively, and t_{ei,i_1} is the beginning time (in units of days) of the first injection, lasting up to t_{ei,i_2}.

Through Eqs. 16 and 17, the temporal evolution t (in units of days) of Γ is assumed from the standard afterglow regime (GS02, [66]):

$$\Gamma(t)_{ISM} = 3.65 \left(\frac{E_{52,k,iso}(t)}{n_0} \right)^{1/8} \left(\frac{t}{z+1} \right)^{-3/8} \tag{18}$$

for ISM-like CBM and

$$\Gamma(t)_{wind} = 3.72 \left(\frac{E_{52,k,iso}(t)}{A_*} \right)^{1/4} \left(\frac{t}{z+1} \right)^{-1/4} \tag{19}$$

for wind-like CBM.

If the energy injection switch is enabled, sAGa works in iterative mode: the first step consists in the MCMC analysis (Sect. 3) of the simple FS (eventually with absorption and/or jet approach) for the data set after $t_{ei,f}$ to determine the micro-physics parameters of the GRB afterglow ($E_{52,k,iso,f}$ included). Successively, these values are assumed as starting point for the energy injection regime at $t < t_{ei,f}$ to obtain the free parameters $t_{ei,i}$ and m (and hence q).

7 Extinction and absorption processes

sAGa accounts for possible dust extinction in optical and photoelectric absorption caused in X-rays (e.g., [72]).

The typical size of dust grains in ISM is comparable to the frequency of blue light. This results in a strong absorption and scattering by the dust grains of the blue light coming from distant objects, making (for an observer on Earth) these objects dimmer (extinction) and redder (reddening) than they really are. GRB afterglows are subject to optical extinction, which is caused by the contribution of (1) the Galactic dust along the line of sight (Galactic) and (2) the dust within the host galaxy (intrinsic). A detailed knowledge of the latter is crucial for (1) determining the intrinsic luminosity of GRB afterglows from X-ray to near-IR frequencies; (2) constraining the nature of the GRB progenitors and their environments; and (3) probing the ISM of high-redshift galaxies and the cosmic star formation history [72]. Nevertheless, dust extinction in GRB host galaxies is still poorly known, and there are different extinction curves that can be assumed to properly model optical afterglow SEDs (e.g. [52, 71, 128, 160]).

sAGa, to determine the extinction A_V (measured in the V band), adopts the extinction curves as parametrised by [98], modelled using Milky Way (MW), or the dust models for Small and Large Magellan Clouds (SMC and LMC, respectively). The extinction correction is not applied to the data set, but only to the modelling and plotting phase.

UV frequencies often are affected by the absorption by neutral hydrogen, from $z \gtrsim 1$. sAGa accounts for this effect through a sight-line-averaged model for the optical depth of the intergalactic medium (IGM) as described by [75], to compute the IGM transmission as a function of wavelength at the redshift of the GRB; this model considers the Lyα absorption by neutral hydrogen along the line of sight and photoelectric absorption by intervening systems. This effect is contained in ETAU_MADAU library of SYNPHOT Python package [129].

Where the X-ray data set are subject to photoelectric absorption, sAGa accounts for this effect through the related hydrogen-equivalent column density N_H (in units of 10^{22} cm^{-2}),

obtained by a polynomial fit of the effective absorption cross-section per hydrogen atom as a function of energy in the 0.03–10 keV range assuming a given abundance pattern [89].

8 Radio interstellar scintillation

Inhomogeneities in the electron density distribution in the MW along the GRB line of sight scatter the flux at low frequencies ($\lesssim 10$ GHz), causing variations in measured flux density of the source. This effect, called interstellar scintillation (ISS), is significant when the source size subtended at the scattering screen is comparable to the size of the inhomogeneities and becomes negligible as the blastwave expands [112, 35, 143, 34, 39]. Usually GRBs show a similar behaviour in their radio light curves, with variations taking place between observations on timescales ranging between hours and days (e.g. [35, 29, 27]). In the standard (and easy) picture, ISS is assumed to take place at a single "thin screen" at some intermediate distance d_{scr} (in units of kpc), typically ~ 1 kpc for high Galactic latitudes.

The strength of the scattering is quantified by a dimensionless parameter, defined as [144]

$$\xi = 7.9 \times 10^3 \mathrm{SM}^{0.6} d_{\mathrm{scr}}^{0.5} \nu_{\mathrm{GHz}}^{-1.7} \, . \tag{20}$$

where SM indicates the scattering measure (in units of kpc m$^{-20/3}$).

There are in general two types of ISS: weak and strong scattering. The weak scattering occurs when $\xi \ll 1$, and the strong scattering regime – in turn divided into refractive and diffractive scintillation – occurs when $\xi \gg 1$ [39]. The transition frequency ν_{trans} between strong and weak ISS is defined as the frequency at which $\xi = 1$ [35]:

$$\nu_{\mathrm{trans}} = 10.4 \ \mathrm{SM}_{-3.5}^{6/17} d_{\mathrm{scr}}^{5/17} \ \mathrm{GHz} \tag{21}$$

where $\mathrm{SM}_{-3.5} = (\mathrm{SM}/10^{-3.5} \ \mathrm{m}^{-20/3} \ \mathrm{kpc})$. ISS depends strongly on frequency: at high radio frequencies only modest flux variations are expected, while at low frequencies strong ISS effects are important. In the strong ISS regime, diffractive scintillation can produce large flux variations on timescales of minutes to hours but is only coherent across a bandwidth $\Delta\nu = (\nu/\nu_{\mathrm{trans}})^{3.4}$ [35, 143].

In all regimes, ξ decreases with time at all frequencies as the size of the emitting region expands, with diffractive ISS suppressing before refractive ISS. The source expansion also increases the typical timescale of the variations for both diffractive and refractive ISS [108]. In this complex situation, the contribution of ISS for each regime is measured by the modulation index m_{scint}, defined as the rms fractional flux density variation. Accurate prescription about the behaviour of m_{scint} is described in [143] and [39], only in the asymptotic regimes ($\xi \ll 1$ for weak ISS and $\xi \gg 1$ for strong ISS), and allows to analyse ISS only in weak/strong refractive or weak/strong diffractive scenario.

sAGa considers the ISS effect through another approach to compute m_{scint}, based on a dedicated fitting function that includes both diffractive and refractive contributions [34]. The values of ν_{trans} and SM are estimated through the NE2001[19] model for the Galactic electron distribution [17]. The expected ISS contribution in the model-predicted flux density F_{model} is defined as (L14):

$$\Delta F_{\mathrm{scint}} = m_{scint} F_{\mathrm{model}} \, . \tag{22}$$

ΔF_{scint} is summed to the uncertainty of flux densities before the MCMC optimisation (Sect. 3); usually this action influences the quality of the radio data set, especially in the

[19] http://www.astro.cornell.edu/~cordes/NE2001/

C-band (4–8 GHz; e.g. [88]), but it is extremely useful to account for the ISS effect in the modelling. Moreover, Eq. (22) is used to highlight the ISS interested range in the spectra and light curves produced by sAGa at the end of the analysis.

9 Inverse-Compton regime

Recently, TeV emission has first been observed from a couple of bright GRB afterglows (190114C, [76]; 180720B, [2]). The SEDs showed a double-peaked shape, with the TeV emission best explained in terms of inverse Compton (IC) up-scattering of synchrotron photons by high-energy electrons. The energies involved in the IC emission – generally occurring when $\epsilon_B \ll \epsilon_e$ – are very large, and hence the ejecta is in a regime in which the IC cross-section decreases rapidly; as a result, a photon undergoes only a single scattering [11, 115, 97, 95, 123].

The contribution of IC emission – in terms of flux density – is typically negligible compared with synchrotron radiation, but the IC mechanism can influence the cooling for the shock-accelerated electrons and hence dominate the total cooling rate (e.g. [123, 155]). The effects of IC depend on the Compton y-parameter[20], defined as

$$y = \frac{-1 + \sqrt{1 + 4\eta\epsilon_e/\epsilon_B}}{2} \tag{23}$$

where η is the fraction of energy that has been radiated away due both to synchrotron and IC radiation. At early-time, during the fast cooling stage of the GRB afterglow, where most of the electron energy is lost, $\eta = 1$ and IC emission dominates over synchrotron; during the slow cooling stage at late-time, η decreases because $\eta = (\nu_c/\nu_m)^{-(p-2)/2}$, and hence the synchrotron component begins to dominate over IC scattering component [123]. Moreover, if $y < 1$, the IC regime can be neglected; otherwise a high-energy component (of the order of 10 MeV) appears in the spectrum and the cooling timescale is shortened by a factor y [123, 102]. As in the case of synchrotron emission, since temporal evolution of the GRB afterglow emission depends on the CBM, IC radiation is different in the case of the ISM-like and wind-like CBM.

sAGa accounts for IC emission by computing y from the FS parameters[21], and hence scaling the spectral break frequencies and flux densities of the synchrotron spectrum by the appropriate powers of $1 + y$ ([123], L14, GS02).

10 Test cases for sAGa

sAGa has been successfully tested on the broadband data of the afterglows of some well studied GRBs (GRB 120521C, GRB 090423, and GRB 050904). Hereafter, we briefly compare the sAGa results with what is reported the literature; our results are consistent with those reported in the literature within $\lesssim 2\sigma$.

10.1 GRB 120521C

GRB 120521C was discovered with the SWIFT/BAT [7] on 2012 May 21 at 23:22:07 UT [8]. This burst is characterised by a duration $T_{90} = (26.7 \pm 0.4)$ s [79] and a high redshift

[20] Note that this equation does not take the Klein–Nishina correction into account [91, 146, 33, 65]. This frequency-dependent correction is expected to be important only at very high frequencies, $\nu \gtrsim 10^{18}$ Hz at $t \gtrsim 1$ d (e.g. [155]). We therefore do not consider this effect further in this analysis.

[21] At the time of writing, this implementation is still work in progress.

Table 2: *Summary statistics from MCMC analysis obtained through the analysis of L14 (first column) and* sAGa *(second column) with broadband data (from radio to X-ray frequencies) of GRB 120521C for a model based on a jetted (sideways-regime) FS emission with optical absorption, in ISM-like CBM.* sAGa *makes use of the χ^2 test to quantify the goodness of fit. Since L14 do not report any statistic that quantifies the goodness of the fit, for comparison we report for L14 the χ^2_r obtained by fixing the parameter set found by those authors. All the uncertainties are reported at 68% (1σ).*

Parameter	Unit	L14	sAGa
p	-	$2.17^{+0.09}_{-0.07}$	2.34 ± 0.07
ϵ_e	-	$(4.5^{+6.7}_{-2.4}) \times 10^{-2}$	$(5.4^{+1.7}_{-1.3}) \times 10^{-2}$
ϵ_B	-	$(7.0^{+0.2}_{-6.0}) \times 10^{-3}$	$(2.4^{+1.3}_{-1.1}) \times 10^{-3}$
n_0	cm^{-3}	$(2.0^{+1.0}_{-0.7}) \times 10^{-3}$	$(6.8^{+4.4}_{-2.8}) \times 10^{-2}$
E_{52}	10^{52} erg	$(2.2^{+3.7}_{-1.4}) \times 10^{1}$	$(2.6^{+4.8}_{-5.9}) \times 10^{1}$
A_v	mag	< 0.05	$(3.1^{+2.1}_{-2.0}) \times 10^{-2}$
t_j	d	$6.8^{+3.8}_{-2.4}$	$3.2^{+2.3}_{-1.3}$
θ_j	deg	$3.0^{+2.3}_{-1.1}$	$3.2^{+0.8}_{-0.6}$
ν_m [a]	Hz	5.5×10^{11}	7.6×10^{11}
ν_c [a]	Hz	1.2×10^{16}	7.4×10^{16}
ν_{sa} [a]	Hz	$\lesssim 5.0 \times 10^{9}$	4.5×10^{8}
ν_{ac} [a]	Hz	-	1.8×10^{10}
χ^2_r	-	1.4	1.1

[a] Measured at $t_{obs} = 1$ d.

($z \approx 6$, L14). The afterglow of GRB 120521C was observed with several facilities from radio to X-rays (VLA, optical/NIR telescopes, SWIFT/XRT) between $\sim 10^{-3}$ d to ~ 200 d after the GRB trigger time, and it is described in terms of FS emission with jet break and dust extinction.

As reported by L14, data prior to 0.25 d are ignored because the X-ray light curve displays a steep decline before ~ 0.01 d, possibly connected to the high-latitude component of the prompt emission (e.g. [63]), followed by a plateau phase extending up to ~ 0.25 d, usually attributed to the energy injection (e.g. [93, 154]). The broadband analysis of the GRB 120521C data after 0.25 d with sAGa, the best-fit model of which is shown in Fig. 3, is compared with the results by L14: in both treatments, an ISM model provides a good fit to the broadband data. As displayed in Table 2, several parameters are consistent with those reported by L14 within $\sim 1\sigma$ (ϵ_e, ϵ_B, E_{52}, A_V, t_j and θ_j), and $\sim 2\sigma$ (p). The self-absorption frequency obtained with sAGa lies below the VLA frequencies, and is therefore not fully constrained; this conclusion is compatible with L14, who also constrained this frequency between 1.75×10^8 Hz and 2.7×10^9 Hz, with our value lying in between (4.5×10^8 Hz).

Finally, the two values of p (Table 2) are also compatible with the one inferred from the optical/X-ray SEDs alone. In this approach, an empirical power-law fit of the optical/X-ray SED at ~ 0.3 d after the explosion yields $\beta = -0.58^{+0.08}_{-0.06}$. At this time the afterglow spectrum is in slow cooling regime ($\nu_m < \nu_c$), resulting in $\beta = (1-p)/2$, and hence $p = 1 - 2\beta = 2.16^{+0.12}_{-0.16}$, compatible with both analyses.

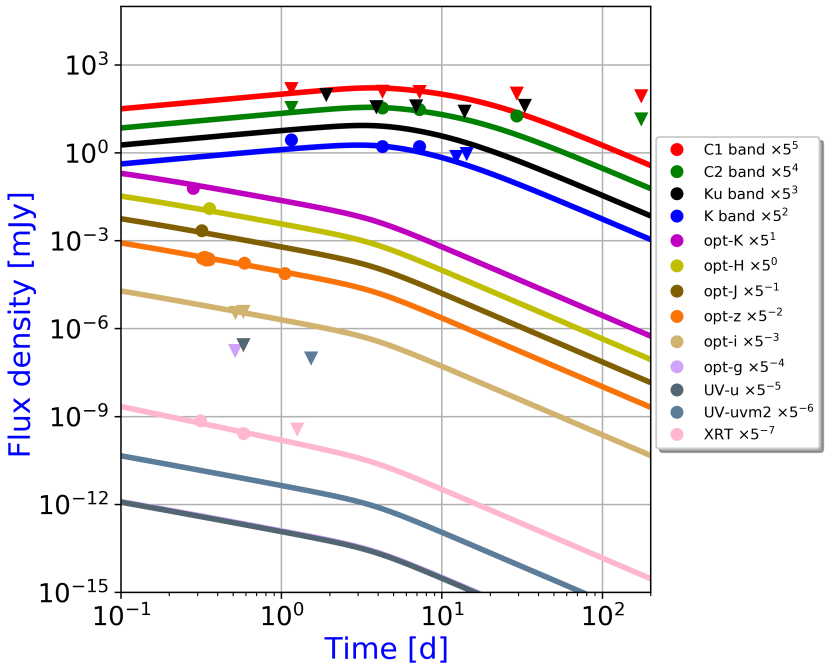

Figure 3: *Broadband modelling of GRB 120521C for a FS model with an ISM-like CBM (GS02). Filled circles indicate detections, and upside down triangles indicate 3σ upper limits. The physical parameters of the burst derived from the best-fit solution are listed in Table 2 (fourth column).*

10.2 GRB 090423

GRB 090423 was discovered with the SWIFT/BAT [7] on 2009 April 23 at 7:55:19 UT [61]. This burst is characterised by a duration $T_{90} = 10.3 \pm 1.1$ s [94] and a high redshift ($z = 8.26$, [116, 132]). The afterglow of GRB 090423 was observed with several facilities from radio to high-energies (VLA, CARMA, optical/NIR telescopes, SWIFT/XRT) between $\sim 10^{-2}$ d to ~ 280 d after the GRB triggering, and it is described in terms of FS, jet break, and dust extinction.

The millimeter data are ignored because they are probably affected by RS radiation (L14). sAGA results are found to agree with those of L14, obtaining a very good fit with an ISM model. We followed the same approach as those authors and fixed the power-law index of the electron energy distribution ($p = 2.56$, based on their best-fit value); our result is in good accordance. Our best-fit model in ISM-like CBM is shown in Fig. 4 and the corresponding physical parameters are listed in Table 3 (third column). Both solutions are consistent with each other within $\sim 1\sigma$. Moreover, thanks to sAGA we estimated that the non-relativistic regime occurs at $t_{NR} = (5.1^{+1.7}_{-1.3}) \times 10^4$ d since the GRB. Finally, the self-absorption frequency ν_{sa} obtained with sAGA is not fully constrained because it lies below the VLA frequencies, compatibly with L14, who also constrained this frequency between 6.8×10^6 Hz and 3.1×10^8 Hz, with my value being 3×10^7 Hz.

The fixed parameter $p = 2.56$ is also compatible with what inferred from optical/X-ray SEDs alone. In this approach, the empirical power-law fit of the optical/X-ray SEDs at 0.07 d and 0.7 d implies $\beta = -0.7 \pm 0.2$. Since the synchrotron spectrum is in slow cooling regime ($\nu_m < \nu_c$) at these epochs, $\beta = (1-p)/2$, and hence $p = 1 - 2\beta = 2.4 \pm 0.4$. Therefore, we analysed the broadband data from GRB 090423 with p as a free parameter, obtaining the results reported in Table 3 (fourth column). Fig. 5 shows our best-fit model in ISM-like

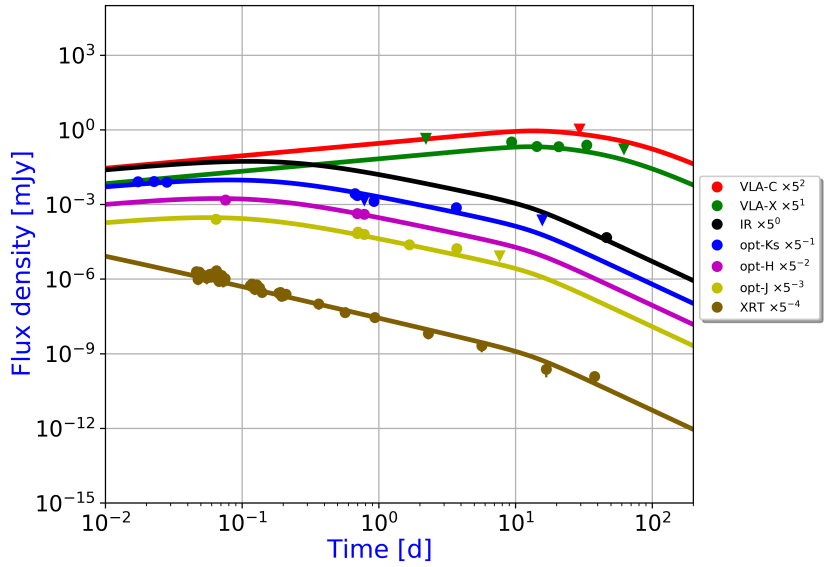

Figure 4: *Broadband modelling of GRB 090423 for a FS model with an ISM-like CBM (GS02), with* $p = 2.56$. *See the caption of Fig. 3 for a full description of the symbols. The physical parameters of the burst derived from the best-fit solution are listed in Table 3 (fourth column).*

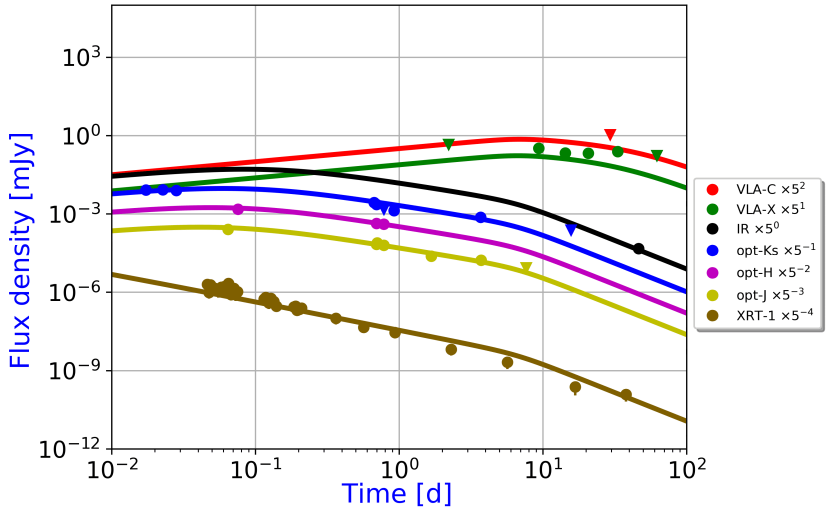

Figure 5: *Broadband modelling of GRB 090423 for a FS model with an ISM-like CBM (GS02), with p as free parameter. See the caption of Fig. 3 for a full description of the symbols. The physical parameters of the burst derived from the best-fit solution are listed in Table 3 (fifth column).*

Table 3: *Summary statistics from the modelling obtained through the analysis of L14 (first column), and* sAGa *(second and third columns) with broadband data (from radio to X-ray frequencies) of GRB 090423 for a model based on a jetted (sideways-regime) FS emission with optical absorption, in ISM-like CBM. The uncertainties are reported at 68% (1σ).*

Parameter	Unit	L14	sAGa	sAGa
p	-	2.56 (fixed)	2.56 (fixed)	$2.31^{+0.17}_{-0.09}$
ϵ_e	-	$(2.7^{+2.0}_{-0.7}) \times 10^{-2}$	$(5.1^{+1.0}_{-0.8}) \times 10^{-2}$	$(3.0^{+1.0}_{-0.4}) \times 10^{-2}$
ϵ_B	-	$(4.8^{+9.5}_{-3.9}) \times 10^{-2}$	$(6.7^{+5.9}_{-3.1}) \times 10^{-3}$	$(2.2^{+0.8}_{-1.7}) \times 10^{-1}$
n_0	cm^{-3}	$(2.5^{+0.6}_{-0.3}) \times 10^{-5}$	$(0.6^{+0.8}_{-0.4}) \times 10^{-5}$	$(4.4^{+6.4}_{-3.1}) \times 10^{-5}$
E_{52}	10^{52} erg	$(3.4^{+1.1}_{-1.4}) \times 10^2$	$(1.8 \pm 0.4) \times 10^2$	$(1.3^{+2.1}_{-0.6}) \times 10^2$
A_v	mag	0.15 ± 0.02	0.11 ± 0.02	$(8.8^{+2.7}_{-1.9}) \times 10^{-2}$
t_j	d	$14.6^{+2.7}_{-2.3}$	13.5 ± 2.7	$7.6^{+5.5}_{-1.5}$
θ_j	deg	$1.5^{+0.7}_{-0.3}$	2.2 ± 0.3	1.3 ± 0.5
ν_m [a]	Hz	7.7×10^{12}	8.1×10^{12}	3.9×10^{12}
ν_c [a]	Hz	4.5×10^{17}	4.9×10^{17}	1.3×10^{16}
ν_{sa} [a]	Hz	$\lesssim 8.0 \times 10^9$	3.0×10^7	1.8×10^8
ν_{ac} [a]	Hz	-	1.0×10^9	2.3×10^9
χ^2_r	-	1.2	0.9	1.3

[a] Measured at $t_{obs} = 1$ d.

CBM. Both solutions are consistent with each other within $\sim 1\sigma$. The non-relativistic regime sets in at $t_{NR} = (1.1 \pm 0.3) \times 10^5$ d after the GRB. Finally, the different value of t_j (and θ_j) obtained through this approach is part of a debate about the presence of jetted emission for this GRB: for example, a previous analysis of GRB 090423 claimed no jet break up to ~ 45 d [14].

10.3 GRB 050904

This GRB was discovered with SWIFT/BAT on 2005 September 4 at 1:51:44 UT [19] and it is characterised by a high redshift ($z = 6.29$, [131, 46, 55]). Broadband data (at radio, optical and X-ray frequencies) are taken from the papers of [36] (hereafter G07) and L14, which describe the GRB afterglow emission in terms of FS, jet break, and dust extinction. Our results are compared with G07 and L14; as in previous studies of this burst ([28], G07 and L14), we find that an ISM model works better than a wind one. Our best-fit model is shown in Fig. 6 and the corresponding physical parameters are listed in Table 4 (third column).

Almost all the parameters obtained with sAGa are consistent with those in the literature within $\sim 1\sigma$ (ϵ_e, A_V, and θ_j) and $\sim 2\sigma$ (ϵ_B, $E_{k,iso,52}$); moreover, we estimated that the non-relativistic regime occurs at $t_{NR} = (4.3^{+1.1}_{-0.9}) \times 10^2$ d after the GRB. The jet break time of $t_j = 3.6$ d inferred by my analysis is later than different values reported in the literature ($t_j = 2.6 \pm 1$ d, [131]; $t_j = 2.63 \pm 0.37$ d, [53]; Table 4), but it is consistent with them within $\sim 2\sigma$.

Finally, our derived value of the p is compatible with the value obtained by G07 within $\sim 2\sigma$, and apparently incompatible with the value obtained by L14. This value, as reported by G07, is explainable through the achromatic break interpretation of GRB afterglow light curves, where the post-jet-break decay index is predicted to be $\alpha = -p$ (Sect. 5); as reported by [131], in the jetted scenario the multiple NIR light curves of the afterglow after t_j are

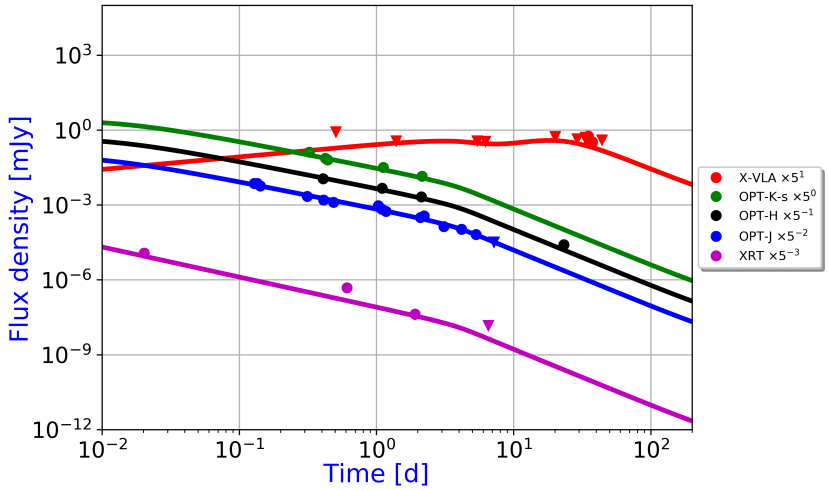

Figure 6: *Broadband modelling of GRB 050904 for a FS model with an ISM-like CBM (GS02). See the caption of Fig. 3 for a full description of the symbols. The physical parameters of the burst derived from the best-fit solution are listed in Table 4 (fifth column).*

described by a decay with power-law index $\alpha = p = 2.4 \pm 0.4$, consistent with the values of p reported in Table 4.

Table 4: *Summary statistics from the modelling obtained through the analysis of G07 (first column), L14 (second column), and* sAGa *(third column) with broadband data (from radio to X-ray frequencies) of GRB 050904 for a model based on a jetted (sideways-regime) FS emission with optical absorption, in ISM-like CBM. All the uncertainties are reported at 68% (1σ).*

Parameter	Unit	G07	L14	sAGa
p	-	2.15 ± 0.04	2.07 ± 0.02	2.29 ± 0.03
ϵ_e	-	$(3.1^{+2.5}_{-1.8}) \times 10^{-2}$	$(1.2^{+1.5}_{-0.5}) \times 10^{-2}$	$(2.5^{+0.6}_{-0.5}) \times 10^{-2}$
ϵ_B	-	$(2.0^{+1.9}_{-1.5}) \times 10^{-1}$	$(1.3^{+2.2}_{-1.1}) \times 10^{-2}$	$(1.3^{+0.5}_{-0.2}) \times 10^{-3}$
n_0	cm^{-3}	$84.4^{+188.6}_{-58.4}$	$(6.3 \pm 0.1) \times 10^2$	$(9.5^{+7.5}_{-3.8}) \times 10^2$
E_{52}	10^{52} erg	$(2.2^{+3.1}_{-0.9}) \times 10^1$	$(1.7^{+1.2}_{-1.0}) \times 10^2$	$(3.5^{+1.1}_{-0.9}) \times 10^1$
A_v	mag	$3.4^{+4.6}_{-1.6} \times 10^{-2}$	< 0.05	$(7.5^{+37.6}_{-5.7}) \times 10^{-4}$
t_j	d	3.2 ± 0.2	$1.5^{+0.2}_{-0.1}$	$3.6^{+0.7}_{-0.4}$
θ_j	deg	$7.3^{+3.0}_{-0.5}$	$6.2^{+3.3}_{-1.4}$	$8.2^{+1.1}_{-0.9}$
ν_m [a]	Hz	-	-	3.7×10^{12}
ν_c [a]	Hz	-	-	3.5×10^{14}
ν_{sa} [a]	Hz	-	-	7.8×10^{10}
ν_{ac} [a]	Hz	-	-	3.4×10^{11}
χ^2_r	-	1.4[b](1.02)[c]	1.4	0.73

[a] Measured at $t_{obs} = 0.1$ d.
[b] Value reported in [36].
[c] This value is obtained with sAGa fixing the parameters to those of G07.

Break frequency	Spectrum	Evolution of break frequency, $\nu \propto t^{\alpha}$					Evolution of flux density, $F_{\nu,b,ext} \propto t^{\beta}$				
		Spherical model		$t > t_{jet}$	$t > t_{NR}$		Spherical model		$t > t_{jet}$	$t > t_{NR}$	
		ISM	Wind		ISM	Wind	ISM	Wind		ISM	Wind
1 - ν_{sa}	1	0	$-3/5$	$-1/5$	$6/5$	$2/15$	$1/2$	$-1/5$	$-2/5$	2	$2/5$
2 - ν_m	1	$-3/2$	$-3/2$	-2	-3	$-7/3$	0	$-1/2$	-1	$3/5$	$-1/3$
3 - ν_c	1,2	$-1/2$	$1/2$	0	$-1/5$	-	$\frac{1-p}{2}$	$\frac{1}{2}-p$	$-p$	$-\frac{10-7p}{5}$	-
4 - ν_m	2,3	$-3/2$	$-3/2$	-2	-3	$-7/3$	$-5/2$	-2	-4	$-32/5$	-4
5 - ν_{sa}	2	$-\frac{3p+2}{2(p+4)}$	$-\frac{3(p+2)}{2(p+4)}$	$-\frac{2(p+1)}{p+4}$	$-\frac{3p-2}{p+4}$	$-\frac{7p+6}{3(p+4)}$	$-\frac{5p-5}{2(p+4)}$	$-\frac{4p+1}{2(p+4)}$	$-\frac{4p+1}{p+4}$	$\frac{47-32p}{5(p+4)}$	$\frac{7-12p}{3(p+4)}$
6 - ν_{sa}	3	$-\frac{3(p+1)}{2(p+5)}$	$-\frac{3p+5}{2(p+5)}$	$-\frac{2(p+1)}{p+5}$	$-\frac{3p-2}{p+4}$	-	$-\frac{5(p-1)}{2(p+5)}$	$-\frac{4p-5}{2(p+5)}$	$-\frac{4p}{p+5}$	-	-
7 - ν_{ac}	4,5	$3/10$	0	$2/5$	-	-	$11/10$	1	$4/5$	-	-
8 - ν_{sa}	4	$-1/2$	$-2/3$	$-2/3$	$6/5$	-	0	$1/12$	$-2/3$	-	-
9 - ν_m	4,5	$-3/2$	$-3/2$	-2	-3	-	$1/2$	$1/2$	0	-	-
10 - ν_{sa}	5	$-1/2$	$-8/5$	$-6/5$	$6/5$	-	0	$-8/5$	$-7/5$	-	-
11 - ν_c	5	$-1/2$	$1/2$	0	$-1/5$	-	0	$-1/2$	-1	-	-

Table 5: *Evolution of spectral break frequencies and peak flux densities – connected with the spectra showed in Fig.* **??** *– before (GS02) and after [120, 122, 96] the jet break and the transition to non-relativistic expansion [30, 139, 70].*

11 Conclusions and future development

This technical note illustrates the Python code sAGa (Software for AfterGlow Analysis), which aims to broadband modelling of GRB afterglows based on an analytical approach.

Built adopting a Bayesian statistics, our code adds up to other pre-existing broadband fitting packages in the literature (e.g. [56, 12, 138, 151, 23, 68, 69, 111, 3, 114, 6]) and provides an independent tool, concerning the broadband study of GRB afterglows over the last two decades. sAGa performs simultaneously a broadband data analysis – from radio to gamma-rays frequencies – in a single iteration through a new approach that consists in the manipulation of all the data both at each observing epoch t_{obs} and observing frequency ν_{obs}, considering different radiation processes and other aspects, described in this technical note. This approach allows the user to estimate in one fell swoop the micro-physics parameters of the GRB afterglow and other physical information that characterises the explosion.

sAGa has been successfully tested on the broadband data set of the afterglows of GRB 120521C, GRB 090423, and GRB 050904. Our results are consistent with those reported in the literature (especially L14, who make use of a similar approach for the characterisation of the GRB afterglow) within $\lesssim 2\sigma$. Moreover, the values of p are compatible with the inferences based on the lines of reasoning based on the observation of the optical/X-ray SEDs.

Another successful application of sAGa concerned the rich and challenging data set of GRB 160131A (Marongiu et al., submit.). Furthermore, the ISS tool has been applied to the radio data set of GRB 190114C [88].

Upon a specific computational improvement and more robust test phase with other sources, sAGa could be even more competitive among the other broadband fitting tools thanks to future implementation of other radiation mechanisms that could contribute to GRB afterglows (IC emission is nearing completion and RS regime is incomplete and currently unavailable). Moreover, other physical aspects could be added, such as more complex jet structures (e.g., either the so-called structured or two-component jet models), and more bumps for energy injection regime (currently sAGa accepts up to two bumps). These improvements are crucial for a future sharing of sAGa with the international community; for further information and collaboration, the reader is encouraged to contact the authors of this technical note.

References

[1] B. P. Abbott, R. Abbott, T. D. Abbott, F. Acernese, K. Ackley, C. Adams, T. Adams, P. Addesso, R. X. Adhikari, V. B. Adya, and et al. Multi-messenger Observations of a Binary Neutron Star Merger. ApJ, 848:L12, October 2017.

[2] H. Abdalla, R. Adam, F. Aharonian, E. O. Ait Benkhali, M. Anguener, C. Arcaro, C. Armand, H. Ashkar, M. Backes, V. Barbosa Martins, M. Barnard Y. Becherini, D. Berge, K. Bernloehr, E. Bissaldi, R. Blackwell, M. Boettcher, C. Boisson, J. Bolmont, S. Bonnefoy, J. Bregeon, M. Breuhaus, F. Brun, P. Brun, M. Bryan, M. Buechele, T. Bulik, T. Bylund, M. Capasso, S. Caroff, A. Carosi, S. Casanova, M. Cerruti, T. Chand, S. Chandra, A. Chen, S. Colafrancesco, M. Curylo, I. D. Davids, C. Deil, J. Devin, P. deWilt, L. Dirson, A. Djannati-Atai, A. Dmytriiev, A. Donath, V. Doroshenko, J. Dyks, K. Egberts, G. Emery, J. P. Ernenwein, S. Eschbach, K. Feijen, S. Fegan, A. Fiasson, G. Fontaine, S. Funk, M. Fuessling, S. Gabici, Y. A. Gallant, F. Gate, G. Giavitto, L. Giunti, D. Glawion, J. F. Glicenstein, D. Gottschall, M. H. Grondin, J. Hahn, M. Haupt, G. Heinzelmann, G. Henri, G. Hermann, J. A. Hinton, W. Hofmann, C. Hoischen, T. L. Holch, M. Holler, D. Horns, D. Huber, H. Iwasaki, M. Jamrozy, D. Jankowsky, F. Jankowsky, A. Jardin-Blicq, I. Jung-Richardt, M. A. Kastendieck, K. Katarzynski, M. Katsuragawa, U. Katz, D. Khangulyan, B. Khelifi, J. King, S. Klepser, W. Kluzniak, N. Komin, K. Kosack, D. Kostunin, M. Kreter, G. Lamanna, A. Lemiere, M. Lemoine-Goumard, J. P. Lenain, E. Leser, C. Levy, T. Lohse, I. Lypova, J. Mackey, J. Majumdar, D. Malyshev, V. Marandon, A. Marcowith, A. Mares, C. Mariaud, G. Marti-Devesa, R. Marx, G. Maurin, P. J. Meintjes, A. M. W. Mitchell, R. Moderski, M. Mohamed, L. Mohrmann, C. Moore, E. Moulin, J. Muller, T. Murach, S. Nakashima, M. de Naurois, H. Ndiyavala, F. Niederwanger, J. Niemiec, L. Oakes, P. O Brien, H. Odaka, S. Ohm, E. de Ona Wilhelmi, M. Ostrowski, I. Oya, M. Panter, R. D. Parsons, C. Perennes, P. O. Petrucci, B. Peyaud, Q. Piel, S. Pita, V. Poireau, A. Priyana Noel, D. A. Prokhorov, H. Prokoph, G. Puehlhofer, M. Punch, A. Quirrenbach, S. Raab, R. Rauth, A. Reimer, O. Reimer, Q. Remy, M. Renaud, F. Rieger, L. Rinchiuso, C. Romoli, G. Rowell, B. Rudak, E. Ruiz-Velasco, V. Sahakian, S. Sailer, S. Saito, D. A. Sanchez, A. Santangelo, M. Sasaki, R. Schlickeiser, F. Schuessler, A. Schulz, H. M. Schutte, U. Schwanke, S. Schwemmer, M. Seglar-Arroyo, M. Senniappan, A. S. Seyffert, N. Shafi, K. Shiningayamwe, R. Simoni, A. Sinha, H. Sol, A. Specovius, M. Spir-Jacob, L. Stawarz, R. Steenkamp, C. Stegmann, C. Steppa, T. Takahashi, T. Tavernier, A. M. Taylor, R. Terrier, D. Tiziani, M. Tluczykont, C. Trichard, M. Tsirou, N. Tsuji, R. Tuffs, Y. Uchiyama, D. J. van der Walt, C. van Eldik, C. van Rensburg, B. van Soelen, G. Vasileiadis, J. Veh, C. Venter, P. Vincent, J. Vink, H. J. Voelk, T. Vuillaume, Z. Wadiasingh, S. J. Wagner, R. White, A. Wierzcholska, R. Yang, H. Yoneda, M. Zacharias, R. Zanin, A. A. Zdziarski, A. Zech, A. Ziegler, J. Zorn, N. Zywucka, F. de Palma, M. Axelsson, and O. J. Roberts. A very-high-energy component deep in the Gamma-ray Burst afterglow. Nature, 575:464–467, Nov 2019.

[3] M. D. Aksulu, R. A. M. J. Wijers, H. J. van Eerten, and A. J. van der Horst. A new approach to modelling {}-ray burst afterglows: Using Gaussian processes to account for the systematics. arXiv e-prints, page arXiv:2004.04166, April 2020.

[4] K. D. Alexander, R. Margutti, P. K. Blanchard, W. Fong, E. Berger, A. Hajela, T. Eftekhari, R. Chornock, P. S. Cowperthwaite, D. Giannios, C. Guidorzi, A. Kathirga-

maraju, A. MacFadyen, B. D. Metzger, M. Nicholl, L. Sironi, V. A. Villar, P. K. G. Williams, X. Xie, and J. Zrake. A Decline in the X-Ray through Radio Emission from GW170817 Continues to Support an Off-axis Structured Jet. ApJ, 863:L18, August 2018.

[5] Astropy Collaboration, T. P. Robitaille, E. J. Tollerud, P. Greenfield, M. Droettboom, E. Bray, T. Aldcroft, M. Davis, A. Ginsburg, A. M. Price-Whelan, W. E. Kerzendorf, A. Conley, N. Crighton, K. Barbary, D. Muna, H. Ferguson, F. Grollier, M. M. Parikh, P. H. Nair, H. M. Unther, C. Deil, J. Woillez, S. Conseil, R. Kramer, J. E. H. Turner, L. Singer, R. Fox, B. A. Weaver, V. Zabalza, Z. I. Edwards, K. Azalee Bostroem, D. J. Burke, A. R. Casey, S. M. Crawford, N. Dencheva, J. Ely, T. Jenness, K. Labrie, P. L. Lim, F. Pierfederici, A. Pontzen, A. Ptak, B. Refsdal, M. Servillat, and O. Streicher. Astropy: A community Python package for astronomy. A&A, 558:A33, October 2013.

[6] Eliot H. Ayache, Hendrik J. van Eerten, and Rupert W. Eardley. GAMMA: a new method for modeling relativistic hydrodynamics and non-thermal emission on a moving mesh. arXiv e-prints, page arXiv:2104.09397, April 2021.

[7] S. D. Barthelmy, L. M. Barbier, J. R. Cummings, E. E. Fenimore, N. Gehrels, D. Hullinger, H. A. Krimm, C. B. Markwardt, D. M. Palmer, A. Parsons, G. Sato, M. Suzuki, T. Takahashi, M. Tashiro, and J. Tueller. The Burst Alert Telescope (BAT) on the SWIFT Midex Mission. Space Sci. Rev., 120:143–164, October 2005.

[8] W. H. Baumgartner, S. D. Barthelmy, D. N. Burrows, M. M. Chester, J. R. Cummings, V. D'Elia, J. A. Kennea, H. A. Krimm, F. E. Marshall, D. M. Palmer, and G. Stratta. GRB 120521C: Swift detection of a burst. GRB Coordinates Network, 13318:1, Jan 2012.

[9] E. Berger, S. R. Kulkarni, G. Pooley, D. A. Frail, V. McIntyre, R. M. Wark, R. Sari, A. M. Soderberg, D. W. Fox, S. Yost, and P. A. Price. A common origin for cosmic explosions inferred from calorimetry of GRB030329. Nature, 426:154–157, November 2003.

[10] Edo Berger. Short-Duration Gamma-Ray Bursts. ARA&A, 52:43–105, Aug 2014.

[11] R. D. Blandford and C. F. McKee. Fluid dynamics of relativistic blast waves. Physics of Fluids, 19:1130–1138, August 1976.

[12] John K. Cannizzo, Neil Gehrels, and Ethan T. Vishniac. A Numerical Gamma-Ray Burst Simulation Using Three-Dimensional Relativistic Hydrodynamics: The Transition from Spherical to Jetlike Expansion. ApJ, 601(1):380–390, Jan 2004.

[13] P. Chandra and D. A. Frail. A Radio-selected Sample of Gamma-Ray Burst Afterglows. ApJ, 746:156, February 2012.

[14] Poonam Chandra, Dale A. Frail, Derek Fox, Shrinivas Kulkarni, Edo Berger, S. Bradley Cenko, Douglas C. J. Bock, Fiona Harrison, and Mansi Kasliwal. Discovery of Radio Afterglow from the Most Distant Cosmic Explosion. ApJ, 712(1):L31–L35, Mar 2010.

[15] Jean-Yves Chenu, Alessandro Navarrini, Yves Bortolotti, Gilles Butin, Anne Laure Fontana, Sylvain Mahieu, Doris Maier, Francois Mattiocco, Patrice Serres, Marylene Berton, Olivier Garnier, Quentin Moutote, Magali Parioleau, Bruno Pissard, and

Julien Reverdy. The Front-End of the NOEMA Interferometer. IEEE Transactions on Terahertz Science and Technology, 6(2):223–237, March 2016.

[16] R. A. Chevalier and Z.-Y. Li. Wind Interaction Models for Gamma-Ray Burst Afterglows: The Case for Two Types of Progenitors. ApJ, 536:195–212, June 2000.

[17] J. M. Cordes and T. J. W. Lazio. NE2001.I. A New Model for the Galactic Distribution of Free Electrons and its Fluctuations. arXiv e-prints, page arXiv:0207156, Jul 2002.

[18] Eric R. Coughlin and Mitchell C. Begelman. Structured, relativistic jets driven by radiation. MNRAS, 499(3):3158–3177, October 2020.

[19] J. Cummings, L. Angelini, S. Barthelmy, A. Cucchiara, N. Gehrels, C. Gronwall, S. T. Holland , V. Mangano, F. Marshall, C. Pagani, and D. Palmer. GRB050904: Swift-BAT detection of a probable burst. GRB Coordinates Network, 3910:1, Jan 2005.

[20] P. A. Curran, R. L. C. Starling, P. T. O'Brien, O. Godet, A. J. van der Horst, and R. A. M. J. Wijers. On the nature of late X-ray flares in Swift gamma-ray bursts. A&A, 487:533–538, August 2008.

[21] Z. G. Dai and T. Lu. γ-Ray Bursts and Afterglows from Rotating Strange Stars and Neutron Stars. Phys. Rev. Lett., 81(20):4301–4304, Nov 1998.

[22] F. Daigne and R. Mochkovitch. Gamma-ray bursts from internal shocks in a relativistic wind: a hydrodynamical study. A&A, 358:1157–1166, June 2000.

[23] Fabio De Colle, Jonathan Granot, Diego López-Cámara, and Enrico Ramirez-Ruiz. Gamma-Ray Burst Dynamics and Afterglow Radiation from Adaptive Mesh Refinement, Special Relativistic Hydrodynamic Simulations. ApJ, 746(2):122, Feb 2012.

[24] M. de Pasquale, P. Evans, S. Oates, M. Page, S. Zane, P. Schady, A. Breeveld, S. Holland, P. Kuin, M. Still, P. Roming, and P. Ward. Jet breaks at the end of the slow decline phase of Swift GRB light curves. MNRAS, 392:153–169, January 2009.

[25] W. Fong, E. Berger, R. Margutti, and B. A. Zauderer. A Decade of Short-duration Gamma-Ray Burst Broadband Afterglows: Energetics, Circumburst Densities, and Jet Opening Angles. ApJ, 815(2):102, Dec 2015.

[26] Daniel Foreman-Mackey, David W. Hogg, Dustin Lang, and Jonathan Goodman. emcee: The MCMC Hammer. PASP, 125(925):306, Mar 2013.

[27] D. A. Frail, E. Berger, T. Galama, S. R. Kulkarni, G. H. Moriarty-Schieven, G. G. Pooley, R. Sari, D. S. Shepherd, G. B. Taylor, and F. Walter. The Enigmatic Radio Afterglow of GRB 991216. ApJ, 538(2):L129–L132, August 2000.

[28] D. A. Frail, P. B. Cameron, M. Kasliwal, E. Nakar, P. A. Price, E. Berger, A. Gal-Yam, S. R. Kulkarni, D. B. Fox, A. M. Soderberg, B. P. Schmidt, E. Ofek, and S. B. Cenko. An Energetic Afterglow from a Distant Stellar Explosion. ApJ, 646(2):L99–L102, Aug 2006.

[29] D. A. Frail, S. R. Kulkarni, L. Nicastro, M. Feroci, and G. B. Taylor. The radio afterglow from the γ-ray burst of 8 May 1997. Nature, 389(6648):261–263, Sep 1997.

[30] D. A. Frail, E. Waxman, and S. R. Kulkarni. A 450 Day Light Curve of the Radio Afterglow of GRB 970508: Fireball Calorimetry. ApJ, 537(1):191–204, Jul 2000.

[31] H. Gao, W.-H. Lei, Y.-C. Zou, X.-F. Wu, and B. Zhang. A Complete Reference of the Analytical Synchrotron External Shock Models of Gamma-Ray Bursts. New Astronomy Reviews, 57:141, December 2013.

[32] H. Gao and P. Mészáros. Relation between the Intrinsic and Observed Central Engine Activity Time: Implications for Ultra-long GRBs. ApJ, 802:90, April 2015.

[33] He Gao, Wei-Hua Lei, Xue-Feng Wu, and Bing Zhang. Compton scattering of self-absorbed synchrotron emission. MNRAS, 435(3):2520–2531, Nov 2013.

[34] J. Goodman and R. Narayan. Fitting Formula for Flux Scintillation of Compact Radio Sources. ApJ, 636(1):510–527, Jan 2006.

[35] Jeremy Goodman. Radio scintillation of gamma-ray-burst afterglows. New A, 2(5):449–460, Nov 1997.

[36] L. J. Gou, D. B. Fox, and P. Mészáros. Modeling GRB 050904: Autopsy of a Massive Stellar Explosion at z=6.29. ApJ, 668(2):1083–1102, Oct 2007.

[37] J. Granot. The Structure and Dynamics of GRB Jets. In Revista Mexicana de Astronomia y Astrofisica, vol. 27, volume 27 of Revista Mexicana de Astronomia y Astrofisica Conference Series, pages 140–165, Mar 2007.

[38] J. Granot, M. Miller, T. Piran, W. M. Suen, and P. A. Hughes. Light Curves from an Expanding Relativistic Jet. In Enrico Costa, Filippo Frontera, and Jens Hjorth, editors, Gamma-ray Bursts in the Afterglow Era, page 312, Jan 2001.

[39] J. Granot and A. J. van der Horst. Gamma-Ray Burst Jets and their Radio Observations. PASA, 31:8, February 2014.

[40] Jonathan Granot, Fabio De Colle, and Enrico Ramirez-Ruiz. Off-axis afterglow light curves and images from 2D hydrodynamic simulations of double-sided GRB jets in a stratified external medium. MNRAS, 481(2):2711–2720, Dec 2018.

[41] Jonathan Granot and Pawan Kumar. Distribution of gamma-ray burst ejecta energy with Lorentz factor. MNRAS, 366(1):L13–L16, Feb 2006.

[42] Jonathan Granot and Tsvi Piran. On the lateral expansion of gamma-ray burst jets. MNRAS, 421(1):570–587, Mar 2012.

[43] Jonathan Granot, Tsvi Piran, and Re'em Sari. The synchrotron spectrum of fast cooling electrons revisited. In R. Marc Kippen, Robert S. Mallozzi, and Gerald J. Fishman, editors, Gamma-ray Bursts, 5th Huntsville Symposium, volume 526 of American Institute of Physics Conference Series, pages 489–493, Sep 2000.

[44] Jonathan Granot and Re'em Sari. The Shape of Spectral Breaks in Gamma-Ray Burst Afterglows. ApJ, 568(2):820–829, Apr 2002.

[45] Yashwant Gupta, H.S. Kale, S. Nayak, S. Sabhapathy, Sureshkumar S., R.V. Swami, Jayaram Chengalur, S.K. Ghosh, C.H. Ishwara-Chandra, Bhal Joshi, Nissim Kanekar, Dharam Lal, and Subhashis Roy. The upgraded gmrt: Opening new windows on the radio universe. Current Science, 113:707–714, 01 2017.

[46] J. B. Haislip, M. C. Nysewander, D. E. Reichart, A. Levan, N. Tanvir, S. B. Cenko, D. B. Fox, P. A. Price, A. J. Castro-Tirado, J. Gorosabel, C. R. Evans, E. Figueredo, C. L. MacLeod, J. R. Kirschbrown, M. Jelinek, S. Guziy, A. de Ugarte Postigo, E. S. Cypriano, A. Lacluyze, J. Graham, R. Priddey, R. Chapman, J. Rhoads, A. S. Fruchter, D. Q. Lamb, C. Kouveliotou, R. A. M. J. Wijers, M. B. Bayliss, B. P. Schmidt, A. M. Soderberg, S. R. Kulkarni, F. A. Harrison, D. S. Moon, A. Gal-Yam, M. M. Kasliwal, R. Hudec, S. Vitek, P. Kubanek, J. A. Crain, A. C. Foster, J. C. Clemens, J. W. Bartelme, R. Canterna, D. H. Hartmann, A. A. Henden, S. Klose, H. S. Park, G. G. Williams, E. Rol, P. O'Brien, D. Bersier, F. Prada, S. Pizarro, D. Maturana, P. Ugarte, A. Alvarez, A. J. M. Fernandez, M. J. Jarvis, M. Moles, E. Alfaro, K. M. Ivarsen, N. D. Kumar, C. E. Mack, C. M. Zdarowicz, N. Gehrels, S. Barthelmy, and D. N. Burrows. A photometric redshift of z = 6.39 ± 0.12 for GRB 050904. Nature, 440(7081):181–183, Mar 2006.

[47] R. Hascoët, F. Daigne, R. Mochkovitch, and V. Vennin. Do Fermi Large Area Telescope observations imply very large Lorentz factors in gamma-ray burst outflows? MNRAS, 421:525–545, March 2012.

[48] Y. F. Huang, X. F. Wu, Z. G. Dai, H. T. Ma, and T. Lu. Rebrightening of XRF 030723: Further Evidence for a Two-Component Jet in a Gamma-Ray Burst. ApJ, 605:300–306, April 2004.

[49] Harold Jeffreys. An Invariant Form for the Prior Probability in Estimation Problems. Proceedings of the Royal Society of London Series A, 186(1007):453–461, Sep 1946.

[50] Eric Jones, Travis Oliphant, Pearu Peterson, et al. SciPy: Open source scientific tools for Python, 2001–. [Online; accessed <today>].

[51] N. Jordana-Mitjans, C. G. Mundell, S. Kobayashi, R. J. Smith, C. Guidorzi, I. A. Steele, M. Shrestha, A. Gomboc, M. Marongiu, R. Martone, V. Lipunov, E. S. Gorbovskoy, D. A. H. Buckley, R. Rebolo, and N. M. Budnev. Lowly Polarized Light from a Highly Magnetized Jet of GRB 190114C. ApJ, 892(2):97, April 2020.

[52] D. A. Kann, S. Klose, and A. Zeh. Signatures of Extragalactic Dust in Pre-Swift GRB Afterglows. ApJ, 641(2):993–1009, Apr 2006.

[53] D. A. Kann, N. Masetti, and S. Klose. The Prompt Optical/Near-Infrared Flare of GRB 050904: The Most Luminous Transient Ever Detected. AJ, 133(3):1187–1192, Mar 2007.

[54] V. K. Kapahi and S. Ananthakrishnan. Astronomy with the Giant Metrewave Radio Telescope (GMRT). Bulletin of the Astronomical Society of India, 23:265, September 1995.

[55] N. Kawai, G. Kosugi, K. Aoki, T. Yamada, T. Totani, K. Ohta, M. Iye, T. Hattori, W. Aoki, H. Furusawa, K. Hurley, K. S. Kawabata, N. Kobayashi, Y. Komiyama, Y. Mizumoto, K. Nomoto, J. Noumaru, R. Ogasawara, R. Sato, K. Sekiguchi, Y. Shirasaki, M. Suzuki, T. Takata, T. Tamagawa, H. Terada, J. Watanabe, Y. Yatsu, and A. Yoshida. An optical spectrum of the afterglow of a γ-ray burst at a redshift of z = 6.295. Nature, 440(7081):184–186, Mar 2006.

[56] S. Kobayashi, T. Piran, and R. Sari. Hydrodynamics of a Relativistic Fireball: The Complete Evolution. ApJ, 513:669–678, March 1999.

[57] S. Kobayashi and R. Sari. Optical Flashes and Radio Flares in Gamma-Ray Burst Afterglow: Numerical Study. ApJ, 542:819–828, October 2000.

[58] S. Kobayashi and B. Zhang. Early Optical Afterglows from Wind-Type Gamma-Ray Bursts. ApJ, 597:455–458, November 2003.

[59] S. Kobayashi and B. Zhang. The Onset of Gamma-Ray Burst Afterglow. ApJ, 655:973–979, February 2007.

[60] D. Kopač, C. G. Mundell, S. Kobayashi, F. J. Virgili, R. Harrison, J. Japelj, C. Guidorzi, A. Melandri, and A. Gomboc. Radio Flares from Gamma-ray Bursts. ApJ, 806:179, June 2015.

[61] H. A. Krimm, A. P. Beardmore, P. A. Evans, O. Godet, C. Gronwall, C. Guidorzi, P. T. O'Brien, K. L. Page, D. M. Palmer, M. Perri, B. Sbarufatti, P. Schady, G. Stratta, G. Tagliaferri, and T. N. Ukwatta. GRB 090423: Swift detection of a burst. GRB Coordinates Network, 9198:1, Jan 2009.

[62] P. Kumar and J. Granot. The Evolution of a Structured Relativistic Jet and Gamma-Ray Burst Afterglow Light Curves. ApJ, 591:1075–1085, July 2003.

[63] Pawan Kumar and Alin Panaitescu. Afterglow Emission from Naked Gamma-Ray Bursts. ApJ, 541(2):L51–L54, Oct 2000.

[64] T. Laskar, K. D. Alexander, E. Berger, W.-f. Fong, R. Margutti, I. Shivvers, P. K. G. Williams, D. Kopač, S. Kobayashi, C. Mundell, A. Gomboc, W. Zheng, K. M. Menten, M. L. Graham, and A. V. Filippenko. A Reverse Shock in GRB 160509A. ApJ, 833:88, December 2016.

[65] T. Laskar, K. D. Alexander, E. Berger, C. Guidorzi, R. Margutti, W.-f. Fong, C. D. Kilpatrick, P. Milne, M. R. Drout, C. G. Mundell, S. Kobayashi, R. Lunnan, R. Barniol Duran, K. M. Menten, K. Ioka, and P. K. G. Williams. First ALMA Light Curve Constrains Refreshed Reverse Shocks and Jet Magnetization in GRB 161219B. ApJ, 862:94, August 2018.

[66] T. Laskar, E. Berger, R. Margutti, D. Perley, B. A. Zauderer, R. Sari, and W.-f. Fong. Energy Injection in Gamma-Ray Burst Afterglows. ApJ, 814:1, November 2015.

[67] T. Laskar, E. Berger, N. Tanvir, B. A. Zauderer, R. Margutti, A. Levan, D. Perley, W.-f. Fong, K. Wiersema, K. Menten, and M. Hrudkova. GRB 120521C at z ˜ 6 and the Properties of High-redshift γ-Ray Bursts. ApJ, 781:1, January 2014.

[68] T. Laskar, E. Berger, B. A. Zauderer, R. Margutti, A. M. Soderberg, S. Chakraborti, R. Lunnan, R. Chornock, P. Chandra, and A. Ray. A Reverse Shock in GRB 130427A. ApJ, 776:119, October 2013.

[69] K. Leventis, A. J. van der Horst, H. J. van Eerten, and R. A. M. J. Wijers. Applying an accurate spherical model to gamma-ray burst afterglow observations. MNRAS, 431(2):1026–1038, May 2013.

[70] K. Leventis, H. J. van Eerten, Z. Meliani, and R. A. M. J. Wijers. Practical flux prescriptions for gamma-ray burst afterglows, from early to late times. MNRAS, 427:1329–1343, December 2012.

[71] Aigen Li, S. L. Liang, D. A. Kann, D. M. Wei, S. Klose, and Y. J. Wang. On Dust Extinction of Gamma-Ray Burst Host Galaxies. ApJ, 685(2):1046–1051, Oct 2008.

[72] Ti-Pei Li. HXMT: A Chinese High-Energy Astrophysics Mission. Nuclear Physics B Proceedings Supplements, 166:131–139, Apr 2007.

[73] E. Liang, B. Zhang, F. Virgili, and Z. G. Dai. Low-Luminosity Gamma-Ray Bursts as a Unique Population: Luminosity Function, Local Rate, and Beaming Factor. ApJ, 662:1111–1118, June 2007.

[74] M. Livio and E. Waxman. Toward a Model for the Progenitors of Gamma-Ray Bursts. ApJ, 538:187–191, July 2000.

[75] Piero Madau. Radiative Transfer in a Clumpy Universe: The Colors of High-Redshift Galaxies. ApJ, 441:18, Mar 1995.

[76] MAGIC Collaboration, V. A. Acciari, S. Ansoldi, L. A. Antonelli, A. Arbet Engels, D. Baack, A. Babić, B. Banerjee, U. Barres de Almeida, J. A. Barrio, J. Becerra González, W. Bednarek, L. Bellizzi, E. Bernardini, A. Berti, J. Besenrieder, W. Bhattacharyya, C. Bigongiari, A. Biland, O. Blanch, G. Bonnoli, Ž. Bošnjak, G. Busetto, R. Carosi, G. Ceribella, Y. Chai, A. Chilingaryan, S. Cikota, S. M. Colak, U. Colin, E. Colombo, J. L. Contreras, J. Cortina, S. Covino, V. D'Elia, P. da Vela, F. Dazzi, A. de Angelis, B. de Lotto, M. Delfino, J. Delgado, D. Depaoli, F. di Pierro, L. di Venere, E. Do Souto Espiñeira, D. Dominis Prester, A. Donini, D. Dorner, M. Doro, D. Elsaesser, V. Fallah Ramazani, A. Fattorini, G. Ferrara, D. Fidalgo, L. Foffano, M. V. Fonseca, L. Font, C. Fruck, S. Fukami, R. J. García López, M. Garczarczyk, S. Gasparyan, M. Gaug, N. Giglietto, N. Giordano, F. andGodinović, D. Green, D. Guberman, D. Hadasch, A. Hahn, J. Herrera, J. Hoang, D. Hrupec, M. Hütten, T. Inada, S. Inoue, K. Ishio, Y. Iwamura, L. Jouvin, D. Kerszberg, H. Kubo, J. Kushida, A. Lamastra, F. Lelas, D. andLeone, E. Lindfors, S. Lombardi, F. Longo, M. López, R. López-Coto, A. López-Oramas, S. Loporchio, B. Machado de Oliveira Fraga, C. Maggio, P. Majumdar, M. Makariev, M. Mallamaci, G. Maneva, M. Manganaro, K. Mannheim, L. Maraschi, M. Mariotti, M. Martínez, D. Mazin, S. Mićanović, D. Miceli, M. Minev, J. M. Mirand a, R. Mirzoyan, E. Molina, A. Moralejo, D. Morcuende, V. Moreno, E. Moretti, P. Munar-Adrover, V. Neustroev, C. Nigro, K. Nilsson, D. Ninci, K. Nishijima, K. Noda, L. Nogués, S. Nozaki, S. Paiano, M. Palatiello, D. Paneque, R. Paoletti, J. M. Paredes, P. Peñil, M. Peresano, M. Persic, P. G. Prada Moroni, E. Prandini, I. Puljak, W. Rhode, M. Ribó, J. Rico, C. Righi, A. Rugliancich, L. Saha, N. Sahakyan, T. Saito, S. Sakurai, K. Satalecka, T. Schmidt, K. andSchweizer, J. Sitarek, I. Šnidarić, D. Sobczynska, A. Somero, A. Stamerra, D. Strom, M. Strzys, Y. Suda, T. Surić, M. Takahashi, F. Tavecchio, P. Temnikov, T. Terzić, M. Teshima, N. Torres-Albà, L. Tosti, V. Vagelli, J. van Scherpenberg, G. Vanzo, M. Vazquez Acosta, C. F. Vigorito, V. Vitale, I. Vovk, M. Will, D. Zarić, L. Nava, P. Veres, P. N. Bhat, M. S. Briggs, W. H. Cleveland, R. Hamburg, C. M. Hui, B. Mailyan, R. D. Preece, O. J. Roberts, A. von Kienlin, C. A. Wilson-Hodge, D. Kocevski, M. Arimoto, D. Tak, K. Asano, M. Axelsson, G. Barbiellini, E. Bissaldi, F. Fana Dirirsa, R. Gill, J. Granot, J. McEnery, N. Omodei, S. Razzaque, F. Piron, J. L. Racusin, D. J. Thompson, S. Campana, M. G. Bernardini, N. P. M. Kuin, M. H. Siegel, S. B. Cenko, P. O'Brien, M. Capalbi, A. Dai, M. de Pasquale, J. Gropp, N. Klingler, J. P. Osborne, M. Perri, R. L. C. Starling, G. Tagliaferri, A. Tohuvavohu, A. Ursi, M. Tavani, M. Cardillo, C. Casentini, G. Piano,

Y. Evangelista, F. Verrecchia, C. Pittori, F. Lucarelli, A. Bulgarelli, N. Parmiggiani, G. E. Anderson, J. P. Anderson, G. Bernardi, J. Bolmer, M. D. Caballero-García, I. M. Carrasco, A. Castellón, N. Castro Segura, A. J. Castro-Tirado, S. V. Cherukuri, A. M. Cockeram, P. D'Avanzo, A. di Dato, R. Diretse, R. P. Fender, E. Fernández-García, J. P. U. Fynbo, A. S. Fruchter, J. Greiner, M. Gromadzki, K. E. Heintz, I. Heywood, A. J. van der Horst, Y. D. Hu, C. Inserra, L. Izzo, V. Jaiswal, P. Jakobsson, J. Japelj, E. Kankare, D. A. Kann, C. Kouveliotou, S. Klose, A. J. Levan, X. Y. Li, S. Lotti, K. Maguire, D. B. Malesani, I. Manulis, M. Marongiu, S. Martin, A. Melandri, M. J. Michałowski, J. C. A. Miller-Jones, K. Misra, A. Moin, K. P. Mooley, S. Nasri, M. Nicholl, A. Noschese, G. Novara, S. B. Pandey, E. Peretti, C. J. Pérez Del Pulgar, M. A. Pérez-Torres, D. A. Perley, L. Piro, F. Ragosta, L. Resmi, R. Ricci, A. Rossi, R. Sánchez-Ramírez, J. Selsing, S. Schulze, S. J. Smartt, I. A. Smith, V. V. Sokolov, J. Stevens, N. R. Tanvir, C. C. Thöne, A. Tiengo, E. Tremou, E. Troja, A. de Ugarte Postigo, A. F. Valeev, S. D. Vergani, M. Wieringa, P. A. Woudt, D. Xu, O. Yaron, and D. R. Young. Observation of inverse Compton emission from a long γ-ray burst. Nature, 575(7783):459–463, Nov 2019.

[77] B. Marcote, K. Nimmo, O. S. Salafia, Z. Paragi, J. W. T. Hessels, E. Petroff, and R. Karuppusamy. Resolving the Decades-long Transient FIRST J141918.9+394036: An Orphan Long Gamma-Ray Burst or a Young Magnetar Nebula? ApJ, 876(1):L14, May 2019.

[78] R. Margutti, F. Genet, J. Granot, R. Barniol Duran, C. Guidorzi, G. Chincarini, J. Mao, P. Schady, T. Sakamoto, A. A. Miller, G. Olofsson, J. S. Bloom, P. A. Evans, J. P. U. Fynbo, D. Malesani, A. Moretti, F. Pasotti, D. Starr, D. N. Burrows, S. D. Barthelmy, P. W. A. Roming, and N. Gehrels. GRB081028 and its late-time afterglow re-brightening. MNRAS, 402:46–64, February 2010.

[79] C. B. Markwardt, S. D. Barthelmy, W. H. Baumgartner, J. R. Cummings, E. E. Fenimore, N. Gehrels, H. A. Krimm, D. M. Palmer, T. Sakamoto, G. Sato, M. Stamatikos, J. Tueller, and T. N. Ukwatta. GRB 120521C: Swift-BAT refined analysis. GRB Coordinates Network, 13333:1, Jan 2012.

[80] M. Marongiu, A. Pellizzoni, E. Egron, T. Laskar, M. Giroletti, S. Loru, A. Melis, G. Carboni, C. Guidorzi, S. Kobayashi, N. Jordana-Mitjans, A. Rossi, C. G. Mundell, R. Concu, R. Martone, and L. Nicastro. Methods for detection and analysis of weak radio sources with single-dish radio telescopes. arXiv e-prints, page arXiv:2004.00346, April 2020.

[81] Jean-Baptiste Marquette. Statistics for Astrophysics: Bayesian Methodology. 2018.

[82] F. E. Marshall, L. A. Antonelli, D. N. Burrows, S. Covino, M. de Pasquale, P. A. Evans, D. Fugazza, S. T. Holland, E. W. Liang, P. T. O'Brien, S. R. Oates, J. P. Osborne, C. Pagani, T. Sakamoto, M. H. Siegel, X. F. Wu, and B. Zhang. The Late Peaking Afterglow of GRB 100418A. ApJ, 727(2):132, Feb 2011.

[83] P. Mészáros. Gamma-ray bursts. Reports on Progress in Physics, 69:2259–2321, August 2006.

[84] P. Meszaros and M. J. Rees. Optical and Long-Wavelength Afterglow from Gamma-Ray Bursts. ApJ, 476:232, February 1997.

[85] P. Mészáros and M. J. Rees. GRB 990123: reverse and internal shock flashes and late afterglow behaviour. MNRAS, 306:L39–L43, July 1999.

[86] B. D. Metzger, D. Giannios, T. A. Thompson, N. Bucciantini, and E. Quataert. The protomagnetar model for gamma-ray bursts. MNRAS, 413:2031–2056, May 2011.

[87] K. Misra, D. Bhattacharya, D. K. Sahu, R. Sagar, G. C. Anupama, A. J. Castro-Tirado, S. S. Guziy, and B. C. Bhatt. Optical observations of GRB 060124 afterglow: a case for an injection break. A&A, 464(3):903–908, Mar 2007.

[88] K. Misra, L. Resmi, D. A. Kann, M. Marongiu, A. Moin, S. Klose, A. de Ugarte Postigo, V. K. Jaiswal, D. A. Perley, A. Ghosh, G. Bernardi, S. Schulze, M. J. Michałowski, S. Martín, A. Cockeram, H. Kumar, S. V. Cherukuri, V. Bhalerao, G. E. Anderson, G. C. Anupama, C. C. Thöne, S. Barway, M. H. Wieringa, J. P. U. Fynbo, and N. Habeeb. Low frequency view of GRB 190114C reveals time varying shock micro-physics. arXiv e-prints, page arXiv:1911.09719, Nov 2019.

[89] R. Morrison and D. McCammon. Interstellar photoelectric absorption cross sections, 0.03-10 keV. ApJ, 270:119–122, July 1983.

[90] C. G. Mundell, A. Melandri, C. Guidorzi, S. Kobayashi, I. A. Steele, D. Malesani, L. Amati, P. D'Avanzo, D. F. Bersier, A. Gomboc, E. Rol, M. F. Bode, D. Carter, C. J. Mottram, A. Monfardini, R. J. Smith, S. Malhotra, J. Wang, N. Bannister, P. T. O'Brien, and N. R. Tanvir. The Remarkable Afterglow of GRB 061007: Implications for Optical Flashes and GRB Fireballs. ApJ, 660:489–495, May 2007.

[91] E. Nakar, S. Ando, and R. Sari. Klein-Nishina Effects on Optically Thin Synchrotron and Synchrotron Self-Compton Spectrum. ApJ, 703:675–691, September 2009.

[92] Ehud Nakar, Tsvi Piran, and Jonathan Granot. The Detectability of Orphan Afterglows. ApJ, 579(2):699–705, Nov 2002.

[93] J. A. Nousek, C. Kouveliotou, D. Grupe, K. L. Page, J. Granot, E. Ramirez-Ruiz, S. K. Patel, D. N. Burrows, V. Mangano, S. Barthelmy, A. P. Beardmore, S. Campana, M. Capalbi, G. Chincarini, G. Cusumano, A. D. Falcone, N. Gehrels, P. Giommi, M. R. Goad, O. Godet, C. P. Hurkett, J. A. Kennea, A. Moretti, P. T. O'Brien, J. P. Osborne, P. Romano, G. Tagliaferri, and A. A. Wells. Evidence for a Canonical Gamma-Ray Burst Afterglow Light Curve in the Swift XRT Data. ApJ, 642(1):389–400, May 2006.

[94] D. M. Palmer, S. D. Barthelmy, W. H. Baumgartner, J. R. Cummings, E. E. Fenimore, N. Gehrels, H. A. Krimm, C. B. Markwardt, A. M. Parsons, T. Sakamoto, G. Sato, M. Stamatikos, J. Tueller, and T. N. Ukwatta. GRB 090423: Swift-BAT refined analysis. GRB Coordinates Network, 9204:1, Jan 2009.

[95] A. Panaitescu and P. Kumar. Analytic Light Curves of Gamma-Ray Burst Afterglows: Homogeneous versus Wind External Media. ApJ, 543:66–76, November 2000.

[96] A. Panaitescu and P. Kumar. Properties of Relativistic Jets in Gamma-Ray Burst Afterglows. ApJ, 571:779–789, June 2002.

[97] A. Panaitescu, P. Meszaros, and M. J. Rees. Multiwavelength Afterglows in Gamma-Ray Bursts: Refreshed Shock and Jet Effects. ApJ, 503:314, August 1998.

[98] Y. C. Pei. Interstellar dust from the Milky Way to the Magellanic Clouds. ApJ, 395:130–139, August 1992.

[99] Fang Peng, Arieh Königl, and Jonathan Granot. Two-Component Jet Models of Gamma-Ray Burst Sources. ApJ, 626(2):966–977, Jun 2005.

[100] D. A. Perley, S. B. Cenko, A. Corsi, N. R. Tanvir, A. J. Levan, D. A. Kann, E. Sonbas, K. Wiersema, W. Zheng, X.-H. Zhao, J.-M. Bai, M. Bremer, A. J. Castro-Tirado, L. Chang, K. I. Clubb, D. Frail, A. Fruchter, E. Göğüş, J. Greiner, T. Güver, A. Horesh, A. V. Filippenko, S. Klose, J. Mao, A. N. Morgan, A. S. Pozanenko, S. Schmidl, B. Stecklum, M. Tanga, A. A. Volnova, A. E. Volvach, J.-G. Wang, J.-M. Winters, and Y.-X. Xin. The Afterglow of GRB 130427A from 1 to 10^{16} GHz. ApJ, 781:37, January 2014.

[101] T. Piran. Gamma-ray bursts and the fireball model. Phys. Rep., 314(6):575–667, Jun 1999.

[102] T. Piran. The physics of gamma-ray bursts. Reviews of Modern Physics, 76:1143–1210, October 2004.

[103] Planck Collaboration, N. Aghanim, Y. Akrami, M. Ashdown, J. Aumont, C. Baccigalupi, M. Ballardini, A. J. Banday, R. B. Barreiro, N. Bartolo, S. Basak, R. Battye, K. Benabed, J. P. Bernard, M. Bersanelli, P. Bielewicz, J. J. Bock, J. R. Bond, J. Borrill, F. R. Bouchet, F. Boulanger, M. Bucher, C. Burigana, R. C. Butler, E. Calabrese, J. F. Cardoso, J. Carron, A. Challinor, H. C. Chiang, J. Chluba, L. P. L. Colombo, C. Combet, D. Contreras, B. P. Crill, F. Cuttaia, P. de Bernardis, G. de Zotti, J. Delabrouille, J. M. Delouis, E. Di Valentino, J. M. Diego, O. Doré, M. Douspis, A. Ducout, X. Dupac, S. Dusini, G. Efstathiou, F. Elsner, T. A. Enßlin, H. K. Eriksen, Y. Fantaye, M. Farhang, J. Fergusson, R. Fernandez-Cobos, F. Finelli, F. Forastieri, M. Frailis, A. A. Fraisse, E. Franceschi, A. Frolov, S. Galeotta, S. Galli, K. Ganga, R. T. Génova-Santos, M. Gerbino, T. Ghosh, J. González-Nuevo, K. M. Górski, S. Gratton, A. Gruppuso, J. E. Gudmundsson, J. Hamann, W. Handley, F. K. Hansen, D. Herranz, S. R. Hildebrandt, E. Hivon, Z. Huang, A. H. Jaffe, W. C. Jones, A. Karakci, E. Keihänen, R. Keskitalo, K. Kiiveri, J. Kim, T. S. Kisner, L. Knox, N. Krachmalnicoff, M. Kunz, H. Kurki-Suonio, G. Lagache, J. M. Lamarre, A. Lasenby, M. Lattanzi, C. R. Lawrence, M. Le Jeune, P. Lemos, J. Lesgourgues, F. Levrier, A. Lewis, M. Liguori, P. B. Lilje, M. Lilley, V. Lindholm, M. López-Caniego, P. M. Lubin, Y. Z. Ma, J. F. Macías-Pérez, G. Maggio, D. Maino, N. Mandolesi, A. Mangilli, A. Marcos-Caballero, M. Maris, P. G. Martin, M. Martinelli, E. Martínez-González, S. Matarrese, N. Mauri, J. D. McEwen, P. R. Meinhold, A. Melchiorri, A. Mennella, M. Migliaccio, M. Millea, S. Mitra, M. A. Miville-Deschênes, D. Molinari, L. Montier, G. Morgante, A. Moss, P. Natoli, H. U. Nørgaard-Nielsen, L. Pagano, D. Paoletti, B. Partridge, G. Patanchon, H. V. Peiris, F. Perrotta, V. Pettorino, F. Piacentini, L. Polastri, G. Polenta, J. L. Puget, J. P. Rachen, M. Reinecke, M. Remazeilles, A. Renzi, G. Rocha, C. Rosset, G. Roudier, J. A. Rubiño-Martín, B. Ruiz-Granados, L. Salvati, M. Sandri, M. Savelainen, D. Scott, E. P. S. Shellard, C. Sirignano, G. Sirri, L. D. Spencer, R. Sunyaev, A. S. Suur-Uski, J. A. Tauber, D. Tavagnacco, M. Tenti, L. Toffolatti, M. Tomasi, T. Trombetti, L. Valenziano, J. Valiviita, B. Van Tent, L. Vibert, P. Vielva, F. Villa, N. Vittorio, B. D. Wand elt, I. K. Wehus, M. White, S. D. M. White, A. Zacchei, and A. Zonca. Planck 2018 results. VI. Cosmological parameters. arXiv e-prints, page arXiv:1807.06209, July 2018.

[104] A. M. Price-Whelan, B. M. Sipőcz, H. M. Günther, P. L. Lim, S. M. Crawford, S. Conseil, D. L. Shupe, M. W. Craig, N. Dencheva, A. Ginsburg, J. T. VanderPlas, L. D. Bradley, D. Pérez-Suárez, M. de Val-Borro, (Primary Paper Contributors, T. L. Aldcroft, K. L. Cruz, T. P. Robitaille, E. J. Tollerud, (Astropy Coordination Committee, C. Ardelean, T. Babej, Y. P. Bach, M. Bachetti, A. V. Bakanov, S. P. Bamford, G. Barentsen, P. Barmby, A. Baumbach, K. L. Berry, F. Biscani, M. Boquien, K. A. Bostroem, L. G. Bouma, G. B. Brammer, E. M. Bray, H. Breytenbach, H. Buddelmeijer, D. J. Burke, G. Calderone, J. L. Cano Rodríguez, M. Cara, J. V. M. Cardoso, S. Cheedella, Y. Copin, L. Corrales, D. Crichton, D. D'Avella, C. Deil, É. Depagne, J. P. Dietrich, A. Donath, M. Droettboom, N. Earl, T. Erben, S. Fabbro, L. A. Ferreira, T. Finethy, R. T. Fox, L. H. Garrison, S. L. J. Gibbons, D. A. Goldstein, R. Gommers, J. P. Greco, P. Greenfield, A. M. Groener, F. Grollier, A. Hagen, P. Hirst, D. Homeier, A. J. Horton, G. Hosseinzadeh, L. Hu, J. S. Hunkeler, Ž. Ivezić, A. Jain, T. Jenness, G. Kanarek, S. Kendrew, N. S. Kern, W. E. Kerzendorf, A. Khvalko, J. King, D. Kirkby, A. M. Kulkarni, A. Kumar, A. Lee, D. Lenz, S. P. Littlefair, Z. Ma, D. M. Macleod, M. Mastropietro, C. McCully, S. Montagnac, B. M. Morris, M. Mueller, S. J. Mumford, D. Muna, N. A. Murphy, S. Nelson, G. H. Nguyen, J. P. Ninan, M. Nöthe, S. Ogaz, S. Oh, J. K. Parejko, N. Parley, S. Pascual, R. Patil, A. A. Patil, A. L. Plunkett, J. X. Prochaska, T. Rastogi, V. Reddy Janga, J. Sabater, P. Sakurikar, M. Seifert, L. E. Sherbert, H. Sherwood-Taylor, A. Y. Shih, J. Sick, M. T. Silbiger, S. Singanamalla, L. P. Singer, P. H. Sladen, K. A. Sooley, S. Sornarajah, O. Streicher, P. Teuben, S. W. Thomas, G. R. Tremblay, J. E. H. Turner, V. Terrón, M. H. van Kerkwijk, A. de la Vega, L. L. Watkins, B. A. Weaver, J. B. Whitmore, J. Woillez, V. Zabalza, and (Astropy Contributors. The Astropy Project: Building an Open-science Project and Status of the v2.0 Core Package. AJ, 156:123, September 2018.

[105] J. L. Racusin, S. V. Karpov, M. Sokolowski, J. Granot, X. F. Wu, V. Pal'Shin, S. Covino, A. J. van der Horst, S. R. Oates, P. Schady, R. J. Smith, J. Cummings, R. L. C. Starling, L. W. Piotrowski, B. Zhang, P. A. Evans, S. T. Holland, K. Malek, M. T. Page, L. Vetere, R. Margutti, C. Guidorzi, A. P. Kamble, P. A. Curran, A. Beardmore, C. Kouveliotou, L. Mankiewicz, A. Melandri, P. T. O'Brien, K. L. Page, T. Piran, N. R. Tanvir, G. Wrochna, R. L. Aptekar, S. Barthelmy, C. Bartolini, G. M. Beskin, S. Bondar, M. Bremer, S. Campana, A. Castro-Tirado, A. Cucchiara, M. Cwiok, P. D'Avanzo, V. D'Elia, M. Della Valle, A. de Ugarte Postigo, W. Dominik, A. Falcone, F. Fiore, D. B. Fox, D. D. Frederiks, A. S. Fruchter, D. Fugazza, M. A. Garrett, N. Gehrels, S. Golenetskii, A. Gomboc, J. Gorosabel, G. Greco, A. Guarnieri, S. Immler, M. Jelinek, G. Kasprowicz, V. La Parola, A. J. Levan, V. Mangano, E. P. Mazets, E. Molinari, A. Moretti, K. Nawrocki, P. P. Oleynik, J. P. Osborne, C. Pagani, S. B. Pandey, Z. Paragi, M. Perri, A. Piccioni, E. Ramirez-Ruiz, P. W. A. Roming, I. A. Steele, R. G. Strom, V. Testa, G. Tosti, M. V. Ulanov, K. Wiersema, R. A. M. J. Wijers, J. M. Winters, A. F. Zarnecki, F. Zerbi, P. Mészáros, G. Chincarini, and D. N. Burrows. Broadband observations of the naked-eye γ-ray burst GRB080319B. Nature, 455:183–188, September 2008.

[106] E. Ramirez-Ruiz and N. M. Lloyd-Ronning. Beam models for gamma-ray bursts sources: outflow structure, kinematics and emission mechanisms. New A, 7:197–210, July 2002.

[107] M. J. Rees and P. Meszaros. Refreshed Shocks and Afterglow Longevity in Gamma-Ray Bursts. ApJ, 496:L1, March 1998.

[108] Lekshmi Resmi. Radio Afterglows of Gamma Ray Bursts. Journal of Astrophysics and Astronomy, 38(3):56, Sep 2017.

[109] J. E. Rhoads. The Dynamics and Light Curves of Beamed Gamma-Ray Burst Afterglows. ApJ, 525:737–749, November 1999.

[110] James E. Rhoads. How to Tell a Jet from a Balloon: A Proposed Test for Beaming in Gamma-Ray Bursts. ApJ, 487(1):L1–L4, September 1997.

[111] L. Rhodes, A. J. van der Horst, R. Fender, I. Monageng, G. E. Anderson, J. Antoniadis, M. F. Bietenholz, M. Bottcher, J. S. Bright, C. Kouveliotou, M. Kramer, S. E. Motta, D. R. A. Williams, P. A. Woudt, and . Radio Afterglows of Very High Energy Gamma-Ray Bursts 190829A and 180720B. arXiv e-prints, page arXiv:2004.01538, April 2020.

[112] B. J. Rickett. Radio propagation through the turbulent interstellar plasma. ARA&A, 28:561–605, Jan 1990.

[113] G. Ryan, H. van Eerten, A. MacFadyen, and B.-B. Zhang. Gamma-Ray Bursts are Observed Off-axis. ApJ, 799:3, January 2015.

[114] Geoffrey Ryan, Hendrik van Eerten, Luigi Piro, and Eleonora Troja. Gamma-Ray Burst Afterglows in the Multimessenger Era: Numerical Models and Closure Relations. ApJ, 896(2):166, June 2020.

[115] G. B. Rybicki and A. P. Lightman. Radiative processes in astrophysics. 1979.

[116] R. Salvaterra, M. Della Valle, S. Campana, G. Chincarini, S. Covino, P. D'Avanzo, A. Fernández-Soto, C. Guidorzi, F. Mannucci, R. Margutti, C. C. Thöne, L. A. Antonelli, S. D. Barthelmy, M. de Pasquale, V. D'Elia, F. Fiore, D. Fugazza, L. K. Hunt, E. Maiorano, S. Marinoni, F. E. Marshall, E. Molinari, J. Nousek, E. Pian, J. L. Racusin, L. Stella, L. Amati, G. Andreuzzi, G. Cusumano, E. E. Fenimore, P. Ferrero, P. Giommi, D. Guetta, S. T. Holland, K. Hurley, G. L. Israel, J. Mao, C. B. Markwardt, N. Masetti, C. Pagani, E. Palazzi, D. M. Palmer, S. Piranomonte, G. Tagliaferri, and V. Testa. GRB090423 at a redshift of z~8.1. Nature, 461(7268):1258–1260, Oct 2009.

[117] R. Santana, R. Barniol Duran, and P. Kumar. Magnetic Fields in Relativistic Collisionless Shocks. ApJ, 785:29, April 2014.

[118] R. Sari and P. Mészáros. Impulsive and Varying Injection in Gamma-Ray Burst Afterglows. ApJ, 535:L33–L37, May 2000.

[119] R. Sari and T. Piran. Predictions for the Very Early Afterglow and the Optical Flash. ApJ, 520:641–649, August 1999.

[120] R. Sari, T. Piran, and J. P. Halpern. Jets in Gamma-Ray Bursts. ApJ, 519:L17–L20, July 1999.

[121] R. Sari, T. Piran, and R. Narayan. Spectra and Light Curves of Gamma-Ray Burst Afterglows. ApJ, 497:L17, April 1998.

[122] Re'em Sari. Gamma Ray Bursts and Their Afterglows. In Philip A. Hughes and Joel N. Bregman, editors, Relativistic Jets: The Common Physics of AGN, Microquasars, and Gamma-Ray Bursts, volume 856 of American Institute of Physics Conference Series, pages 33–56, Sep 2006.

[123] Re'em Sari and Ann A. Esin. On the Synchrotron Self-Compton Emission from Relativistic Shocks and Its Implications for Gamma-Ray Burst Afterglows. ApJ, 548(2):787–799, Feb 2001.

[124] S. Schulze, S. Klose, G. Björnsson, P. Jakobsson, D. A. Kann, A. Rossi, T. Krühler, J. Greiner, and P. Ferrero. The circumburst density profile around GRB progenitors: a statistical study. A&A, 526:A23, February 2011.

[125] Sanjib Sharma. Markov Chain Monte Carlo Methods for Bayesian Data Analysis in Astronomy. ARA&A, 55(1):213–259, August 2017.

[126] L. Sironi, U. Keshet, and M. Lemoine. Relativistic Shocks: Particle Acceleration and Magnetization. Space Sci. Rev., 191:519–544, October 2015.

[127] Lorenzo Sironi, Anatoly Spitkovsky, and Jonathan Arons. The Maximum Energy of Accelerated Particles in Relativistic Collisionless Shocks. ApJ, 771(1):54, Jul 2013.

[128] G. Stratta, S. Gallerani, and R. Maiolino. Is GRB 050904 at z = 6.3 absorbed by dust? A&A, 532:A45, Aug 2011.

[129] STScI development Team. synphot: Synthetic photometry using Astropy, Nov 2018.

[130] G. Swarup. Giant metrewave radio telescope (GMRT) - Scientific objectives and design aspects. Indian Journal of Radio and Space Physics, 19:493–505, December 1990.

[131] G. Tagliaferri, L. A. Antonelli, G. Chincarini, A. Fernández-Soto, D. Malesani, M. Della Valle, P. D'Avanzo, A. Grazian, V. Testa, S. Campana, S. Covino, F. Fiore, L. Stella, A. J. Castro-Tirado, J. Gorosabel, D. N. Burrows, M. Capalbi, G. Cusumano, M. L. Conciatore, V. D'Elia, P. Filliatre, D. Fugazza, N. Gehrels, P. Goldoni, D. Guetta, S. Guziy, E. V. Held, K. Hurley, G. L. Israel, M. Jelínek, D. Lazzati, A. López-Echarri, A. Melandri, I. F. Mirabel, M. Moles, A. Moretti, K. O. Mason, J. Nousek, J. Osborne, L. J. Pellizza, R. Perna, S. Piranomonte, L. Piro, A. de Ugarte Postigo, and P. Romano. GRB 050904 at redshift 6.3: observations of the oldest cosmic explosion after the Big Bang. A&A, 443(1):L1–L5, Nov 2005.

[132] N. R. Tanvir, D. B. Fox, A. J. Levan, E. Berger, K. Wiersema, J. P. U. Fynbo, A. Cucchiara, T. Krühler, N. Gehrels, J. S. Bloom, J. Greiner, P. A. Evans, E. Rol, F. Olivares, J. Hjorth, P. Jakobsson, J. Farihi, R. Willingale, R. L. C. Starling, S. B. Cenko, D. Perley, J. R. Maund, J. Duke, R. A. M. J. Wijers, A. J. Adamson, A. Allan, M. N. Bremer, D. N. Burrows, A. J. Castro-Tirado, B. Cavanagh, A. de Ugarte Postigo, M. A. Dopita, T. A. Fatkhullin, A. S. Fruchter, R. J. Foley, J. Gorosabel, J. Kennea, T. Kerr, S. Klose, H. A. Krimm, V. N. Komarova, S. R. Kulkarni, A. S. Moskvitin, C. G. Mundell, T. Naylor, K. Page, B. E. Penprase, M. Perri, P. Podsiadlowski, K. Roth, R. E. Rutledge, T. Sakamoto, P. Schady, B. P. Schmidt, A. M. Soderberg, J. Sollerman, A. W. Stephens, G. Stratta, T. N. Ukwatta, D. Watson, E. Westra, T. Wold, and C. Wolf. A γ-ray burst at a redshift of z~8.2. Nature, 461(7268):1254–1257, Oct 2009.

[133] A. R. Thompson, B. G. Clark, C. M. Wade, and P. J. Napier. The Very Large Array. ApJS, 44:151–167, October 1980.

[134] Tomonori Totani and Alin Panaitescu. Orphan Afterglows of Collimated Gamma-Ray Bursts: Rate Predictions and Prospects for Detection. ApJ, 576(1):120–134, Sep 2002.

[135] Z. Lucas Uhm, Bing Zhang, Romain Hascoët, Frédéric Daigne, Robert Mochkovitch, and Il H. Park. Dynamics and Afterglow Light Curves of Gamma-Ray Burst Blast Waves with a Long-lived Reverse Shock. ApJ, 761(2):147, Dec 2012.

[136] A. J. van der Horst, A. Kamble, L. Resmi, R. A. M. J. Wijers, D. Bhattacharya, B. Scheers, E. Rol, R. Strom, C. Kouveliotou, T. Oosterloo, and C. H. Ishwara-Chandra. Detailed study of the GRB 030329 radio afterglow deep into the non-relativistic phase. A&A, 480(1):35–43, Mar 2008.

[137] H. van Eerten, A. van der Horst, and A. MacFadyen. Gamma-Ray Burst Afterglow Broadband Fitting Based Directly on Hydrodynamics Simulations. ApJ, 749:44, April 2012.

[138] H. van Eerten, W. Zhang, and A. MacFadyen. Off-axis Gamma-ray Burst Afterglow Modeling Based on a Two-dimensional Axisymmetric Hydrodynamics Simulation. ApJ, 722:235–247, October 2010.

[139] H. J. van Eerten, K. Leventis, Z. Meliani, R. A. M. J. Wijers, and R. Keppens. Gamma-ray burst afterglows from transrelativistic blast wave simulations. MNRAS, 403(1):300–316, Mar 2010.

[140] H. J. van Eerten and A. I. MacFadyen. Gamma-Ray Burst Afterglow Scaling Relations for the Full Blast Wave Evolution. ApJL, 747:L30, March 2012.

[141] Hendrik van Eerten. Self-similar relativistic blast waves with energy injection. MNRAS, 442(4):3495–3510, Aug 2014.

[142] Hendrik J. van Eerten and Andrew I. MacFadyen. Synthetic Off-axis Light Curves for Low-energy Gamma-Ray Bursts. ApJ, 733(2):L37, Jun 2011.

[143] Mark A. Walker. Interstellar scintillation of compact extragalactic radio sources. MNRAS, 294:307–311, Feb 1998.

[144] Mark A. Walker. Erratum: Interstellar scintillation of compact extragalactic radio sources. MNRAS, 321(1):176–176, Feb 2001.

[145] Xiang-Gao Wang, Bing Zhang, En-Wei Liang, Rui-Jing Lu, Da-Bin Lin, Jing Li, and Long Li. Gamma-Ray Burst Jet Breaks Revisited. ApJ, 859(2):160, Jun 2018.

[146] Xiang-Yu Wang, Hao-Ning He, Zhuo Li, Xue-Feng Wu, and Zi-Gao Dai. Klein-Nishina Effects on the High-energy Afterglow Emission of Gamma-ray Bursts. ApJ, 712(2):1232–1240, Apr 2010.

[147] E. Waxman. Angular Size and Emission Timescales of Relativistic Fireballs. ApJ, 491:L19, December 1997.

[148] Ralph A. M. J. Wijers, Martin J. Rees, and Peter Meszaros. Shocked by GRB 970228: the afterglow of a cosmological fireball. Monthly Notices of the Royal Astronomical Society, 288(4):L51–L56, Jul 1997.

[149] S. E. Woosley and J. S. Bloom. The Supernova Gamma-Ray Burst Connection. ARAA, 44:507–556, September 2006.

[150] X. F. Wu, Z. G. Dai, Y. F. Huang, and T. Lu. Gamma-ray bursts: polarization of afterglows from two-component jets. MNRAS, 357(4):1197–1204, Mar 2005.

[151] N. Wygoda, E. Waxman, and D. A. Frail. Relativistic Jet Dynamics and Calorimetry of Gamma-ray Bursts. ApJ, 738(2):L23, September 2011.

[152] B. Zhang. The Physics of Gamma-Ray Bursts. Cambridge University Press, 2019.

[153] B. Zhang, X. Dai, N. M. Lloyd-Ronning, and P. Mészáros. Quasi-universal Gaussian Jets: A Unified Picture for Gamma-Ray Bursts and X-Ray Flashes. ApJ, 601:L119–L122, February 2004.

[154] B. Zhang, Y. Z. Fan, J. Dyks, S. Kobayashi, P. Mészáros, D. N. Burrows, J. A. Nousek, and N. Gehrels. Physical Processes Shaping Gamma-Ray Burst X-Ray Afterglow Light Curves: Theoretical Implications from the Swift X-Ray Telescope Observations. ApJ, 642:354–370, May 2006.

[155] B. Zhang, E. Liang, K. L. Page, D. Grupe, B.-B. Zhang, S. D. Barthelmy, D. N. Burrows, S. Campana, G. Chincarini, N. Gehrels, S. Kobayashi, P. Mészáros, A. Moretti, J. A. Nousek, P. T. O'Brien, J. P. Osborne, P. W. A. Roming, T. Sakamoto, P. Schady, and R. Willingale. GRB Radiative Efficiencies Derived from the Swift Data: GRBs versus XRFs, Long versus Short. ApJ, 655:989–1001, February 2007.

[156] Bin-Bin Zhang, Hendrik van Eerten, David N. Burrows, Geoffrey Scott Ryan, Philip A. Evans, Judith L. Racusin, Eleonora Troja, and Andrew MacFadyen. An Analysis of Chandra Deep Follow-up Gamma-Ray Bursts: Implications for Off-axis Jets. ApJ, 806(1):15, Jun 2015.

[157] Bing Zhang and Peter Mészáros. Gamma-Ray Burst Afterglow with Continuous Energy Injection: Signature of a Highly Magnetized Millisecond Pulsar. ApJ, 552(1):L35–L38, May 2001.

[158] Bing Zhang and Peter Mészáros. Gamma-Ray Burst Beaming: A Universal Configuration with a Standard Energy Reservoir? ApJ, 571(2):876–879, Jun 2002.

[159] Weiqun Zhang and Andrew MacFadyen. The dynamics and afterglow radiation of gamma-ray bursts. i. constant density medium. ApJ, 698(2):1261, 2009.

[160] Alberto Zonca, Cesare Cecchi-Pestellini, Giacomo Mulas, Silvia Casu, and Giambattista Aresu. Modeling Extragalactic Extinction through Gamma-Ray Burst Afterglows. ApJ, 829(1):22, Sep 2016.

[161] Y. C. Zou, X. F. Wu, and Z. G. Dai. Estimation of the detectability of optical orphan afterglows. A&A, 461(1):115–119, January 2007.

[162] J. T. L. Zwart, R. W. Barker, P. Biddulph, D. Bly, R. C. Boysen, A. R. Brown, C. Clementson, M. Crofts, T. L. Culverhouse, J. Czeres, R. J. Dace, M. L. Davies, R. D'Alessandro, P. Doherty, K. Duggan, J. A. Ely, M. Felvus, F. Feroz, W. Flynn, T. M. O. Franzen, J. Geisbüsch, R. Génova-Santos, K. J. B. Grainge, W. F. Grainger, D. Hammett, R. E. Hills, M. P. Hobson, C. M. Holler, N. Hurley-Walker, R. Jilley, M. E. Jones, T. Kaneko, R. Kneissl, K. Lancaster, A. N. Lasenby, P. J. Marshall, F. Newton, O. Norris, I. Northrop, D. M. Odell, G. Petencin, J. C. Pober, G. G. Pooley, M. W. Pospieszalski, V. Quy, C. Rodríguez-Gonzálvez, R. D. E. Saunders, A. M. M.

Scaife, J. Schofield, P. F. Scott, C. Shaw, T. W. Shimwell, H. Smith, A. C. Taylor, D. J. Titterington, M. Velić, E. M. Waldram, S. West, B. A. Wood, G. Yassin, and AMI Consortium. The Arcminute Microkelvin Imager. MNRAS, 391(4):1545–1558, December 2008.